June 2019

On Distributed Control of Multiagent Systems under Adverse Conditions

Emre Yildirim
University of South Florida, yildirimemre1453@hotmail.com

On Distributed Control of Multiagent Systems under Adverse Conditions

by

Emre Yildirim

A thesis submitted in partial fulfillment
of the requirements for the degree of
Master of Science in Mechanical Engineering
Department of Mechanical Engineering
College of Engineering
University of South Florida

Major Professor: Tansel Yucelen, Ph.D.
Kyle Reed, Ph.D.
Yasin Yilmaz, Ph.D.

Date of Approval:
June 17, 2019

Keywords: Control with local information exchange, Adaptive control, Control under limited resources, Stability analysis

DEDICATION

I am wholeheartedly dedicating this thesis to my beloved parents, Fatma and Huseyin, who continually provide their love, support, and encouragement to me. This thesis is also dedicated to my lovely wife, Hatice, for her kindness, devotion, and emotional support as well as to my wonderful sister, Esra.

ACKNOWLEDGMENTS

I would like to take this opportunity to express my gratitude to the people who helped me through completing this work successfully. I would first like to express my sincere gratitude to my advisor, Dr. Tansel Yucelen, for his never-ending support, guidance, and immense knowledge. His enthusiasm and perfection in doing research was always inspiring and motivational for me, which attracted me to accomplish my studies willingfully and immaculately. I am particularly grateful to the other members of my Ph.D. committee, Dr. Kyle Reed and Dr. Yasin Yilmaz, for their time and helpful comments. I would also wish to thank Dr. Rasim Guldiken for helpful guidance through the graduate school process.

I would also like to offer my special thanks to Dr. Brendan Nagle for his patient guidance, encouragement, invaluable knowledge and willingness to give his extra time so generously to me during the course of graph theory. In addition, I would like to acknowledge the financial support from the Republic of Turkey Ministry of National Education.

I am also grateful for the invaluable experience, I have had with my fellow labmates at the University of South Florida. I would like to thank S. Burak Sarsilmaz, K. Merve Dogan, Dr. Benjamin Gruenwald, Dzung Tran, Dr. Ehsan Arabi, Dr. Ahmet T. Koru, Jesse Jaramillo, Kevin Wilcher, Stefan Ristevski, Mehdi Madani, Benjamin Rigsby, and Fatemeh Rasouli. In addition, I would like to offer my special thanks to S. Burak Sarsilmaz for his great guidance, extraordinary help and inspiring critiques, which have been invaluable for me.

Finally, I would like to thank my parents, my sister, and my wife. Without their love, support, and encouragement, I would not have finished my master education successfully.

TABLE OF CONTENTS

LIST OF TABLES

LIST OF FIGURES

ABSTRACT

The objective of this thesis is (1) to show the experimental validation of recently proposed distributed adaptive control architecture for a class of heterogeneous uncertain multiagent systems as well as (2) to theoretically propose a proportional integral controller for multiagent systems having limited resources in the presence of a disturbance with stability analyses.

With regard to (1), the distributed adaptive control architecture used in the experiment utilizes a control input having a nominal part and an adaptive augmentation part for each agent to suppress the effect of uncertainties and disturbances effectively. This architecture is capable to provide uniform ultimate boundedness for the output tracking error between each heterogeneous uncertain agent and the leader with unknown dynamics. In addition, if the output of the leader converges to a constant, then the output of each agent asymptotically converges to the output of the leader by this architecture, where the system is subject to matched disturbances and time-invariant system uncertainties over fixed (i.e., time-invariant) and directed graph topology. The experimental setup for validating this architecture is a multiagent mechanical platform composed of two-cart inverted pendulums and a cart. In order to achieve heterogeneity, two carts are attached with different length of pendulums and a cart is used without pendulum. Our mechanical platform involves uncertainties due to friction between pinions of carts and the track. It is observed during the experimental process that the output of agents follow the output of the leader with huge amplitude of oscillations comparing to the control input with adaptive augmentation. This adaptive augmentation minimizes the effect of uncertainties and make the output of agents follow the output of the leader with considerably lower amplitude of oscillations. Several experimental plots are also given to show the efficacy of the proposed distributed adaptive control architecture.

We now summarize (2). In contrast to the control architecture used, for example (1), in some real-life scenarios it is not cost-effective to implement a controller into each agent. To address this problem, a proportional integral controller is proposed to implement only one control input into the multiagent system, which is composed of agents executing the distributed information based on the graph topology

in the presence of a disturbance (i.e., cyber-attack or malfunction) through only an agent (i.e., driver agent) to robustify the overall closed-loop multiagent system. To this end, the trajectories of all agents in the multiagent system with a fixed, connected and undirected graph, where the system subject to a bounded disturbance through an agent (i.e., misbehaving agent), remain bounded with only one control input having a bounded command irrespective of which agent we apply the control input. After that, we introduce two methods to derive the steady-state value of each agent in the multiagent system whose graph topology for the first method is fixed, connected and undirected and for the second method is a fixed, connected, and undirected acyclic graph. While the second method is applicable to only the acyclic graph, it does not require an inverse of a matrix dependent on the graph topology. The second approach also shows that the largest steady-state deviation from the desired command in the multiagent system is minimized if the driver agent is located as close as possible to the misbehaving agent. Several numerical examples are also presented to illustrate the implementation of the theoretical results.

CHAPTER 1: INTRODUCTION

Multiagent systems consist of large teams of agents that locally communicate with each other, execute the distributed information, and work cooperatively based on the graph topology. These systems have been an attractive research topic in the systems and control community over the last two decades after the developments in communication, sensor, and computer technologies. In addition, multiagent systems have attracted growing attention from diverse fields owing to the wide interest in their applications such as microsatellite clusters, sensor networks, unmanned vehicles, mobile robots, and automated highway systems. In the literature, multiagent systems composed of agents having identical dynamics (respectively, non-identical dynamics) are called homogeneous multiagent systems (respectively, heterogenous multiagent systems).

With respect to controlling multiagent systems, two approaches generally adopted in the control systems literature; that is, a centralized approach and a distributed approach. The motivation behind the centralized approach is that each agent in the system is capable of reaching the central controller, which is sufficiently powerful to navigate the whole system. On the other hand, distributed approach does not require a central station at the expense of making the system more complexed in terms of structure and organization [2]. Due to many physical constraints such as the possibility of communication bandwidth restrictions on the information exchange between agents, energy constraints to name but a few, distributed sensing and control is required in the real-life applications of multiagent systems [3]. Therefore, theoretical outcomes and challenges mostly emerge from controlling these systems through partial and relative information (i.e., distributed control) without using a central controller (i.e., centralized control) [4]. In what follows, we first provide a concise overview of distributed control algorithms.

1.1 Distributed Control

The distributed control is a method to control multiagent systems that utilizes information exchange between neighbor agents based on a graph topology in order to achieve a given objective. It has several

advantages in terms of attaining the overall common behavior such as less operational expenses, less system requirements, and higher flexibility in scalability [2].

The system theoretic advancements in distributed control of multiagent systems has played a critical role in controlling multiagent systems in order to address problems such as achieving consensus, formation, and containment objectives. Consensus control can be considered in two categories; that is, leaderless consensus and leader-follower consensus. Leaderless consensus means that each agent eventually reach a common value [5], [6]. On the other hand, leader-follower consensus (i.e., consensus tracking) is a cooperative task navigated by a leader. In particular, it is desired that the state of each agent converges to the trajectory produced by using the single leader [3], [7]. Containment control arises if there exists multiple leaders in the multiagent system to drive other agents to a safe region (i.e., convex hull) spanned by leaders [8], [9]. Formation control accounts for the manipulation of agents to generate and maintain a desired geometric shape [10], [11]. Note that the main difference between consensus, containment and formation controls is the final states, which each agent eventually reach.

In practical applications, multiagent systems are generally subject to disturbances and uncertainties such as modeling errors, frictions, actuator bias, and system nonlinearities. One of major issues the local controller encounters is stability of each agent in the multiagent system under disturbances and uncertainties as well as performing the overall system objective. To this end, distributed adaptive control is a strong tool to maintain the stability of the multiagent systems in the presence of disturbances and uncertainties (e.g., see [12], [13], [14]). As a class of multiagent systems, heterogeneous multiagent systems under nonidentical system uncertainties and disturbances are also investigated since agents cannot perform their distributed control approaches identically and this may lead to instability of the controlled multiagent systems (e.g., see [14, 15] and references therein).

This thesis demonstrates the experimental validation of recently proposed distributed adaptive control architecture in [15] on a heterogeneous mechanical platform composed of two cart-inverted pendulums and a cart to show the efficacy of this architecture in practice. It has been shown that the output of each agent follows the output of the leader with smaller amplitude of oscillations by turning on the adaptive augmentation on, as desired. The performance gets worse when we turn the adaptive augmentation off (i.e., only nominal part). We presents experimental plots to show the efficacy of the proposed distributed adaptive control architecture.

1.2 Multiagent Systems with Limited Resources

Technological advancements in networking and the production of electromechanical systems in a miniature scale made the use of distributed control laws possible to control large scale systems. Due to the lack of monitoring and controlling each agent in the multiagent system, agents in the system become susceptible to cyber-attacks and malfunctions [16]. In the control systems literature, there exists numerous studies considering cases, where each agent in the system is supposed to be subject to a disturbance. For these cases, each agent is equipped with controllers, which are resisting to adverse conditions [17], [18]. However, this approach is not cost-effective for some real-life applications.

Specifically, consider sensor networks as an example for large scale systems, which are susceptible to have malfunctioning sensors. Sensor networks consist of a large number of low-cost, small battery-powered, and wireless sensors, which are densely placed in the environment to take measurements and transfer the data to a central processor. Due to the restrictions on size and energy, these low-cost sensors have limited capabilities in terms of processing, data transfer and storage. Some sensors may stop working or function improperly and send false information into the network if these sensors are subject to adverse environmental conditions, hardware or software failures [19]. When a sensor begins to malfunction, it (i.e., misbehaving agent) relays false information into the network and this results in moving the whole system in the direction of the faulty sensor value [20]. If each sensor is equipped with controllers, which are capable of suppressing the effect of a disturbance, the stated problems can be overcome. However, this is not desirable since this will increase the cost of each sensor dramatically, which are used in high number.

In this thesis, we shows that the trajectories of all agents stay bounded if the multiagent system having a fixed, connected, and undirected graph topology is subject to a bounded disturbance through an agent (i.e., misbehaving agent) by using only a control input having a bounded command irrespective of which agent we apply the control input. This reduces the necessity of making each agent equipped with advanced controllers, which are resisting to disturbances. In addition, the steady-state value of each agent is derived based on the control input is applied to the undisturbed and disturbed agent, respectively. Finally, we derive a graph-theoretical approach to show explicitly the steady-state value of each agent in the multiagent system having a fixed, connected, and undirected graph topology. This approach shows that the largest steady-state deviation from the desired command in the multiagent system is minimized if the driver agent

is located as close as possible to the misbehaving agent. We then present numerical examples to depict the implementation of these theoretical results.

1.3 Main Contributions

The main contributions of this thesis are to demonstrate (1) the experimental validation of recently proposed distributed adaptive control architecture in [15] on a heterogeneous mechanical platform composed of two cart-inverted pendulums and a cart to show the efficacy of this architecture in practice, (2) the stability analysis of multiagent systems having a fixed, connected and undirected graph topology in the presence of a disturbance without and with a control input, and (3) two methods to derive the steady-state value of each agent in the multiagent system whose graph topology for the first method is fixed, connected and undirected and for the second method is a fixed, connected, and undirected acyclic graph. Also, the second method shows that the largest steady-state deviation from the desired command in the multiagent system is minimized if the driver agent is located as close as possible to the misbehaving agent.

1.4 Organization

The organization of this thesis is as follows. Chapter 2 presents an experimental study on a heterogeneous multiagent mechanical platform to show the efficacy of the proposed distributed controller in [15]. Chapter 3 proposes a proportional integral controller to robustify the overal closed-loop multiagent system subject to a disturbance with limited resources. After that, we introduce two methods to derive the steady-state value of each agent in the multiagent system whose graph topology for the first method is fixed, connected and undirected and for the second method is a fixed, connected, and undirected acyclic graph. In addition, the second method is used to show how to minimize the largest steady-state deviation from the desired command in the multiagent system based on locating the driver agent with respect to the misbehaving agent. Finally, concluding remarks and future research directions are presented in Chapter 4.

CHAPTER 2: APPLICATION OF A DISTRIBUTED ADAPTIVE CONTROL APPROACH TO A HETEROGENEOUS MULTIAGENT MECHANICAL PLATFORM[1]

A distributed adaptive control architecture is recently developed for a class of heterogeneous uncertain multiagent systems [15]. This architecture has the capability to provide uniform ultimate boundedness for the output tracking error between each heterogeneous uncertain agent and the leader with unknown dynamics. As a special case, in addition, it allows the output of agents to asymptotically converge to the output of the leader, which converges to a constant, in the presence of matched disturbances and time-invariant system uncertainties over fixed and directed communication graph topologies. The main contribution of this paper is to provide an experimental study on a heterogeneous multiagent mechanical platform composed of two cart-inverted pendulums and a cart to demonstrate the performance of this architecture in practice.

2.1 Introduction

Multiagent systems are composed of agents having either same dynamics (called homogeneous multiagent systems) or different dynamics (called heterogeneous multiagent systems). Controlling these systems in a distributed fashion is a highly attractive and active research topic since it includes a wide array of applications such as unmanned aerial vehicles, spacecraft, mobile robots; to name but a few examples. Over the last two decades, these systems have been studied by many researchers; however, the number of experimental implementations into many applications is considerably less than the number of papers related to theoretical studies and contributions in this field. The main contribution of this paper is to provide an experimental study on a heterogeneous multiagent mechanical platform based on a distributed control algorithm recently developed by the authors of [15].

On background and literature related to distributed control of heterogeneous multiagent systems, we refer to [15]. We now outline the key aspects of the new distributed control algorithm presented in [15].

[1]This chapter is previously published in [21]. Permission is included in Appendix B.

Specifically, the algorithm in [15] is proposed for a group of heterogeneous uncertain multiagent systems with a leader having unknown dynamics over fixed and directed communication graph topologies. First, the uniform ultimate boundedness of the output tracking error between the output of the reference model of each agent and the output of the leader is theoretically demonstrated. If, in addition, the output of the leader is either constant or converges to a constant, then the output tracking error goes to zero as time goes to infinity (Theorem 1, [15]). Second, an agent-wise local sufficient stability condition is presented (Theorem 2, [15]). Finally, an adaptive controller is designed due to the possible existence of matched system uncertainties and unknown external disturbances. In this part of [15], uniform ultimate boundedness

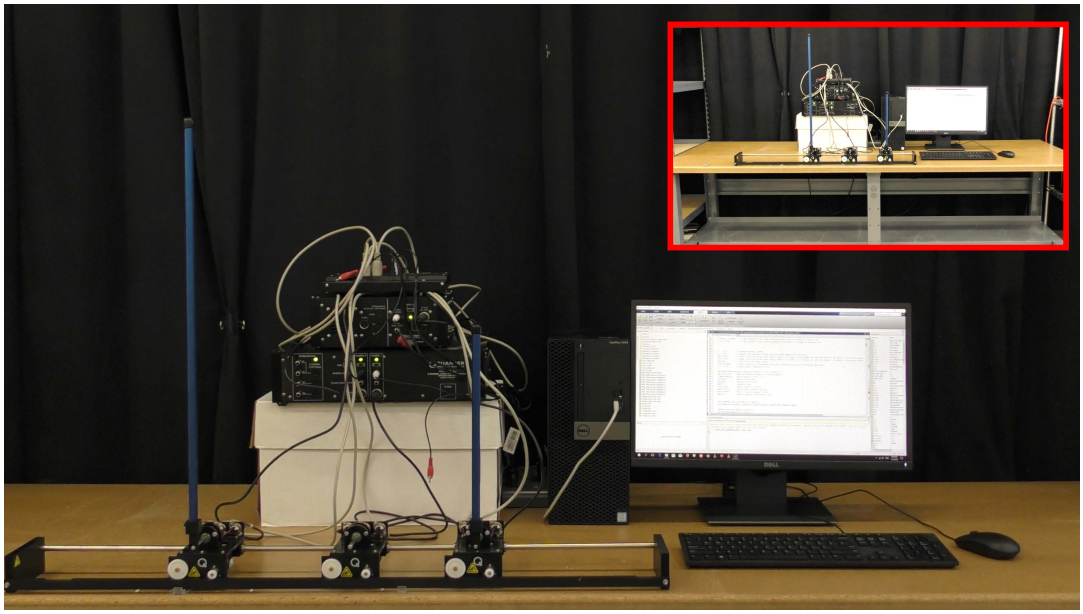

Figure 2.1: Considered heterogeneous multiagent mechanical platform.

of the output tracking error between the output of the reference model of each agent and the output of the corresponding agent is shown. If there exist no unmatched external disturbances for any agent in the graph and the system uncertainties are time-invariant, then the output of the reference model of each agent is tracked by the output of each agent asymptotically (Theorem 3, [15]). A concise summary of the sufficient conditions and assumptions for satisfying those theorems are given later in this paper to be self-contained.

In this paper, we provide an experimental study on a heterogeneous multiagent mechanical platform. In particular, this platform is composed of two cart-inverted pendulums and a cart, and is used to demonstrate the distributed adaptive control approach of [15] in practice. Figure 2.1 shows this platform, where the cart-

inverted pendulum on the left represents the first agent, the cart in the middle represents the second agent, and the cart-inverted pendulum on the right represents the third agent. They clearly form a heterogeneous multiagent system since the cart in the middle has second-order dynamics, whereas the first and third cart-inverted pendulums have fourth-order dynamics. Moreover, while the first and third cart-inverted pendulums share the same order, the long and small pendulums on these carts make them heterogeneous in dynamics. We present modeling, dynamical equations, and respective control design of this system later in this paper.

2.2 Mathematical Preliminaries

We follow the notation of [15] in this paper. To be self-contained, the set of real numbers is shown by $\mathbb{R}$, the set of $n \times 1$ real column vectors is shown by $\mathbb{R}^n$, the set of $n \times m$ real matrices is shown by $\mathbb{R}^{n\times m}$, and the $n \times n$ identity matrix is shown by I_n. Furthermore, $\rho(\cdot)$ denotes the spectral radius of a square matrix, $(\cdot)^{\mathrm{T}}$ denotes the transpose of a matrix, $(\cdot)^{-1}$ denotes the inverse of a nonsingular matrix, $\|\cdot\|_2$ denotes the (induced) 2-norm of a matrix, $\|\cdot\|_{\mathrm{F}}$ denotes the Frobenius norm of a matrix, diag$(\cdot)$ denotes block diagonal function, and "$\triangleq$" denotes equality by definition. Finally, we can define the set of all piecewise continuous functions $u : [0,\infty) \to \mathbb{R}^m$ such that $\|u(t)\|_{\mathcal{L}_2} = \left(\int_0^\infty \|u(t)\|_2^2 \mathrm{dt}\right)^{1/2} < \infty$ as the space $\mathcal{L}_2$ [22].

Based on [23], which is adopted in [15], we next highlight the necessary notations related to the graph theory. Consider a fixed (i.e., time-invariant) directed graph $\mathcal{G} = (V,E)$ with $V = \{v_1,\ldots,v_N\}$ being a nonempty finite set of N nodes and $E \subset V \times V$ being a set of edges. Specifically, each node in V corresponds to an agent in the network. There is an edge rooted at node v_j and ended at v_i, i.e., $(v_j,v_i) \in E$, if and only if v_i receives information from v_j. $A = [a_{ij}] \in \mathbb{R}^{N\times N}$ denotes the adjacency matrix describing the graph structure; in other words, $a_{ij} = 1$ if and only if $(v_j,v_i) \in E$ (and $a_{ij} = 0$ otherwise). Repeated edges and self loops are not allowed in this paper ($a_{ii} = 0,\ \forall i \in \mathcal{N}$ with $\mathcal{N} = \{1,\ldots,N\}$). The set of neighbors of node v_i is denoted as $N_i = \{j|(v_j,v_i) \in E\}$. In-degree matrix is defined as $D = \mathrm{diag}(d_1,\ldots,d_N)$ with $d_i = \sum_{j\in N_i} a_{ij}$. In addition, a directed path from node v_i to node v_j is a sequence of successive edges in the form $\{(v_i,v_p),(v_p,v_q),\ldots,(v_r,v_j)\}$, where a directed graph is said to have a spanning tree when there is a root node such that it has directed paths to all other nodes in the graph. We denote the fixed augmented directed graph by $\bar{\mathcal{G}} = (\bar{V},\bar{E})$ with $\bar{V} = \{v_0,v_1,\ldots,v_N\}$ being the set of $N+1$ nodes, including the leader node v_0 and all nodes in V, and $\bar{E} = E \cup E'$ is the set of edges with E' consisting of some edges in the form of (v_0,v_i), $i \in \mathcal{N}$.

Finally, we state the projection operator used in the results of this paper, where we refer to, for example, [24], [15] for details. Specifically, let $f:\mathbb{R}^n \longrightarrow \mathbb{R}$ be a continuously differentiable convex function given by $f(\theta) \triangleq \frac{(1+\varepsilon_\theta)\theta^{\mathrm{T}}\theta-\theta_{\max}^2}{\varepsilon_\theta \theta_{\max}^2}$, where $\theta_{\max}>0$ being the projection norm bound; that is $\|\theta\|_2 \leq \theta_{\max}$. The projection tolerance is denoted as $\varepsilon_\theta > 0$ and we can define the projection operator as

$$\mathrm{Proj}(\theta,y) \triangleq \begin{cases} \left(I_n - \frac{f(\theta)}{(\nabla f(\theta))^{\mathrm{T}}\Gamma\nabla f(\theta)}\Gamma\nabla f(\theta)(\nabla f(\theta))^{\mathrm{T}}\right)y & \text{if } f(\theta)>0 \text{ and } y^{\mathrm{T}}\nabla f(\theta)>0, \\ y, & \text{otherwise,} \end{cases} \tag{2.1}$$

with $y \in \mathbb{R}^n$, $\Gamma \in \mathbb{R}^{n\times n}$ being a positive-definite matrix, and $\nabla f(\theta) = \frac{2(1+\varepsilon_\theta)}{\varepsilon_\theta \theta_{\max}^2}\theta$. The projection operator can be implemented in a matrix form as,

$$\mathrm{Proj}_{\mathrm{m}}(\Theta,Y) = (\mathrm{Proj}(\mathrm{col}_1(\Theta),\mathrm{col}_1(Y)),\ldots,\mathrm{Proj}(\mathrm{col}_m(\Theta),\mathrm{col}_m(Y))), \tag{2.2}$$

with $\Theta \in \mathbb{R}^{n\times m}, Y \in \mathbb{R}^{n\times m}$, and $\mathrm{col}_j(\cdot)$ being jth column operator. For convenience, it is assumed that $\theta_{\max}$ is the projection norm bound on each column of $\Theta \in \mathbb{R}^{n\times m}$. Once again, we refer to, for example, [24], [15] for the properties associated with the projection operator given by (2.1) and by (2.2).

2.3 Problem Setup

In Sections 2.3 and 2.4, the essential parts presented in [15] are concisely summarized in order to pave the way for bridging theoretical aspect of [15] and the experimental results of this paper. To begin with, a set of N agents is considered, which have heterogeneous uncertain dynamics over a fixed and directed communication graph topology $\mathcal{G}$ with the dynamics of each agent i satisfying

$$\dot{x}_i(t) = A_i x_i(t) + B_i[u_i(t)+\Delta_i(t,x_i(t))] + \delta_i(t), \quad x_i(t_0)=x_{i0}, \quad t \geq t_0, \tag{2.3}$$

$$y_i(t) = C_i x_i(t). \tag{2.4}$$

Here, $x_i(t) \in \mathbb{R}^{n_i}$ denotes the state, $u_i(t) \in \mathbb{R}^{m_i}$ denotes the input, $y_i(t) \in \mathbb{R}^l$ denotes the output, $A_i \in \mathbb{R}^{n_i\times n_i}$ denotes the known system matrix, $B_i \in \mathbb{R}^{n_i\times m_i}$ denotes the known input matrix, and $C_i \in \mathbb{R}^{l\times n_i}$ denotes the known output matrix. Furthermore, $\Delta_i : [t_0,\infty)\times\mathbb{R}^{n_i} \to \mathbb{R}^{m_i}$ represents a matched system uncertainty and $\delta_i(t) \in \mathbb{R}^{n_i}$ stands for possible unknown external disturbances. To be consistent with the

results presented in [15], the following assumptions are given for matched system uncertainty and unknown external disturbances.

Assumption 1 (Structured Uncertainty Parameterization). The time-varying and state dependent matched system uncertainty in (2.3) is linearly parameterized as $\Delta_i(t,x_i) = W_i^{\mathrm{T}}(t)\sigma_i(x_i), \quad x_i \in \mathbb{R}^{n_i}$. Here, $W_i(t) \in \mathbb{R}^{s_i \times m_i}$ denotes the unknown time-varying weight matrix whose columns bounded (i.e.,$\|\mathrm{col}_j W_i(t)\|_2 \leq \frac{W_{\mathrm{max}i}}{\sqrt{1+\varepsilon_\theta}},\ j = 1,\ldots,m_i,\ \forall t \geq t_0,\ \forall i \in \mathcal{N}$), and its derivative is piecewise continuous and bounded (i.e., $\|\dot{W}_i(t)\|_{\mathrm{F}} \leq \dot{w}_i,\ \forall t \geq t_0,\ \forall i \in \mathcal{N}$). In addition, $\sigma : \mathbb{R}^{n_i} \rightarrow \mathbb{R}^{s_i}$ denotes a known basis function of the form $\sigma_i(x_i) = [\sigma_{i1}(x_i),\ldots,\sigma_{is_i}(x_i)]^{\mathrm{T}}$ with its components being locally Lipschitz in x_i. Finally, one can write $\|W_i(t)\|_{\mathrm{F}} \leq w_i,\ w_i = \sqrt{\frac{m_i}{1+\varepsilon_\theta}} W_{\mathrm{max}i},\ \forall t \geq t_0,\ \forall i \in \mathcal{N}$.

Assumption 2 (Boundedness of the Disturbance). There exists a nonnegative constant α_i such that $\|\delta_i(t)\|_2 \leq \alpha_i < \infty, \forall t \geq t_0, \forall i \in \mathcal{N}$.

Next, note that the unknown dynamics of the leader can be either linear or nonlinear with any dimension under the circumstances of having a unique solution. Now, we define the output tracking error as

$$e_i(t) \triangleq y_i(t) - y_0(t). \tag{2.5}$$

with $y_i(t) \in \mathbb{R}^l$ and $y_0(t) \in \mathbb{R}^l$ being the output of the ith agent and the leader, respectively. If an agent v_i receives information from the leader v_0, an edge (v_0,v_i) with weighting gain $k_i = 1$ exists; otherwise, $k_i = 0$.

Finally, the objective of [15] is to make the output tracking error between the leader and each agent uniformly ultimately bounded through establishing a distributed adaptive control architecture $u_i(t)$. In addition, the output of each agent asymptotically converges to the output of the leader if the unknown weight matrix is constant, the basis function has a bias term, unmatched external disturbances do not exist, and either the output of the leader is constant or it converges to a constant vector. In order to accomplish this objective, the following assumptions[1] are made in [15].

Assumption 3 (Boundedness of the Output of the Leader and its Derivative). There exist nonnegative constants β and $\dot{\beta}$ such that $\|y_0(t)\|_2 \leq \beta < \infty$ and $\|\dot{y}_0(t)\|_2 \leq \dot{\beta} < \infty$ for all $t \geq t_0$.

Assumption 4 (Connectedness of the Augmented Graph). The augmented graph $\bar{\mathcal{G}}$ has a spanning tree, where the leader node is the root node.

[1] With the approach in [25], Assumption 5 becomes redundant. However, we keep it in this paper to be consistent with the presentation of [15].

Assumption 5 (Nonsingular Matrix Conditions). There exist K_{1i} and K_{2i} such that $A_{\mathrm{m}i} \triangleq A_i - B_iK_{1i} \in \mathbb{R}^{n_i \times n_i}$ and $B_{\mathrm{m}i} \triangleq -B_iK_{2i} \in \mathbb{R}^{n_i \times l}$ with $A_{\mathrm{m}i}$ and $C_iA_{\mathrm{m}i}^{-1}B_{\mathrm{m}i}$ being nonsingular for all $i \in \mathcal{N}$.

Assumption 6 (Stabilizability). For all $i \in \mathcal{N}$, the pair (A_i, B_i) is stabilizable.

Assumption 7 (A Rank Condition). Each agent satisfies rank $\begin{bmatrix} A_i & B_i \\ C_i & 0 \end{bmatrix} = n_i + l$.

2.4 Distributed Control Algorithm

2.4.1 Reference Model Design

We now summarize the reference model design presented in [15], which utilizes $(y_{\mathrm{r}i}(t) - y_{\mathrm{r}j}(t))$ for all $j \in N_i$. Mathematically speaking, dynamics of the reference model of each agent i is given by

$$\dot{x}_{\mathrm{r}i}(t) = A_{\mathrm{m}i}x_{\mathrm{r}i}(t) + B_{\mathrm{m}i}z_{\mathrm{r}i}(t), \quad x_{\mathrm{r}i}(t_0) = x_{\mathrm{r}i0}, \quad t \geq t_0, \tag{2.6}$$

$$\dot{z}_{\mathrm{r}i}(t) = \frac{1}{d_i + k_i}\Big[\sum_{j \in N_i} a_{ij}\big(y_{\mathrm{r}i}(t) - y_{\mathrm{r}j}(t)\big) + k_i\big(y_{\mathrm{r}i}(t) - y_0(t)\big)\Big], \quad z_{\mathrm{r}i}(t_0) = z_{\mathrm{r}i0}, \quad t \geq t_0, \tag{2.7}$$

$$y_{\mathrm{r}i}(t) = C_ix_{\mathrm{r}i}(t). \tag{2.8}$$

Here, $x_{\mathrm{r}i}(t) \in \mathbb{R}^{n_i}$ denotes the reference state, $z_{\mathrm{r}i}(t) \in \mathbb{R}^l$ denotes the reference integrator state, and $y_{\mathrm{r}i}(t) \in \mathbb{R}^l$ denotes the reference output. For notational convenience, we define

$$e_{\mathrm{r}i}(t) \triangleq y_{\mathrm{r}i}(t) - y_0(t), \tag{2.9}$$

as the output tracking error between the output of each reference model and the output of the leader.

Remark 1 (Global Sufficient Stability Condition for $e_{\mathrm{r}i}(t)$) (**Theorem 1,** [15]). Let Assumptions 3, 4 and 5 hold. If the resulting closed-loop system matrix is Hurwitz, then Theorem 1 of [15] guarantees that $e_{\mathrm{r}i}(t)$ is uniformly ultimately bounded for all $i \in \mathcal{N}$. If, in addition, the output of the leader is a constant or $\lim_{t\to\infty} y_0(t) = r^\star \in \mathbb{R}^l$ ($r^\star$ is finite) and $\dot{y}_0(t)$ is uniformly continuous on $[0,\infty)$ or $\lim_{t\to\infty} \dot{y}_0(t) = 0$, then one can also conclude that $\lim_{t\to\infty} e_{\mathrm{r}i}(t) = 0$, $\forall i \in \mathcal{N}$.

In practice, it is also important to have an agent-wise local sufficient condition that yields the resulting closed-loop system matrix being Hurwitz. Once again, following the results in [15], we now provide a summary on this point. For this purpose, let $\xi_{\mathrm{r}i}(t) \triangleq \big[x_{\mathrm{r}i}^{\mathrm{T}}(t), z_{\mathrm{r}i}^{\mathrm{T}}(t)\big]^{\mathrm{T}}$ for all $i \in \mathcal{N}$ and $F \triangleq \mathrm{diag}\Big(\frac{1}{d_1+k_1}, \ldots, \frac{1}{d_N+k_N}\Big)$. We can then write the dynamics of each reference model given by (2.6) and (2.7)

as

$$\dot{\xi}_{ri}(t) \quad = \quad (\bar{A}_i - \bar{B}_i\bar{K}_i)\xi_{ri}(t) + B_{fi}\mu_i(t), \quad \xi_{ri}(t_0) = \xi_{ri0}, \quad t \geq t_0. \tag{2.10}$$

Here, $\bar{A}_i = \begin{bmatrix} A_i & 0 \\ C_i & 0 \end{bmatrix}$, $\bar{B}_i = \begin{bmatrix} B_i \\ 0 \end{bmatrix}$, $\bar{K}_i = [K_{1i},\ K_{2i}]$, $B_{fi} = \begin{bmatrix} 0 \\ -I_l \end{bmatrix}$, and $\mu_i(t) = \frac{1}{d_i+k_i}\left[\sum_{j\in N_i} a_{ij}y_{rj}(t) + k_i y_0(t)\right]$.
We can also restate the dynamics of each reference model with the output equation as

$$\dot{\xi}_{ri}(t) \quad = \quad A_{fi}\xi_{ri}(t) + B_{fi}\mu_i(t), \quad \xi_{ri}(t_0) = \xi_{ri0}, \quad t \geq t_0, \tag{2.11}$$

$$y_{ri}(t) \quad = \quad C_{fi}\xi_{ri}(t), \tag{2.12}$$

with $A_{fi} = \begin{bmatrix} A_{mi} & B_{mi} \\ C_i & 0 \end{bmatrix}$ and $C_{fi} = [C_i,\ 0]$. One can now write

$$g_i(s) = C_{fi}(sI - A_{fi})^{-1}B_{fi}, \tag{2.13}$$

which denotes the transfer matrix from $\mu_i(t)$ to $y_{ri}(t)$. From [15] and (Lemma 1.26, [26]), there always exist such K_{1i} and K_{2i} for ensuring A_{fi} being Hurwitz by Assumptions 6 and 7. If A_{fi} is Hurwitz for each agent in $\mathcal{G}$, then the system given in (2.11) and (2.12) is $\mathcal{L}_2$ stable with finite gain (Theorem 5.4, [22])

$$\gamma_i = \sup_{\omega\in\mathbb{R}} \|g_i(j\omega)\|_2 < \infty, \quad \forall i \in \mathcal{N}. \tag{2.14}$$

Remark 2 (Agent-wise Local Sufficient Stability Condition) [25], [27]. Let Assumption 4 hold and A_{fi} be Hurwitz for all $i \in \mathcal{N}$. Then, the resulting closed loop system matrix obtained from (2.6), (2.7) and (2.8) is Hurwitz when

$$\gamma_i\rho(FA) < 1, \quad \forall i \in \mathcal{N}. \tag{2.15}$$

2.4.2 Adaptive Controller Design

Next, a concise overview of the adaptive control design in [15] is given. In particular, define

$$\tilde{y}_i(t) \quad \triangleq \quad y_i(t) - y_{ri}(t), \tag{2.16}$$

as the output tracking error, which is between the output of each agent and the output of each corresponding reference model. To demonstrate the uniform ultimate boundedness of the output tracking error between each agent and the leader, the uniform ultimate boundedness of $\tilde{y}_i(t)$ is first shown. To this end, each agent in $\mathcal{G}$ is assumed to have access to $\big(y_i(t)-y_{\mathrm{r}j}(t)\big)$ for all $j\in N_i$, where the controller of an agent has the form

$$u_i(t)=\underbrace{-K_{1i}x_i(t)-K_{2i}z_i(t)}_{u_{\mathrm{n}i}(t)}\underbrace{-\hat{W}_i^{\mathrm{T}}(t)\sigma_i(x_i(t))}_{u_{\mathrm{ad}i}(t)}. \tag{2.17}$$

Here, $u_{\mathrm{n}i}(t)$ denotes the nominal controller and it is augmented by $u_{\mathrm{ad}i}(t)$, which stands for the adaptive controller. Moreover, $\hat{W}_i(t)\in\mathbb{R}^{s_i\times m_i}$ denotes the estimate of $W_i(t)$ and $z_i(t)\in\mathbb{R}^l$ denotes the integrator state. Letting $\tilde{W}_i(t)\triangleq W_i(t)-\hat{W}_i(t)$, one can equivalently rewrite (2.3) as

$$\dot{x}_i(t) \;=\; A_{\mathrm{m}i}x_i(t)+B_{\mathrm{m}i}z_i(t)+B_i\tilde{W}_i^{\mathrm{T}}(t)\sigma_i(x_i(t))+\delta_i(t),\quad x_i(t_0)=x_{i0},\quad t\geq t_0, \tag{2.18}$$

under the Assumption 1 with utilizing the controller $u_i(t)$ in (2.17). In addition, the dynamics of the integrator satisfies

$$\dot{z}_i(t) \;=\; \frac{1}{d_i+k_i}\Big[\sum_{j\in N_i}a_{ij}\big(y_i(t)-y_{\mathrm{r}j}(t)\big)+k_i\big(y_i(t)-y_0(t)\big)\Big],\quad z_i(t_0)=z_{i0},\quad t\geq t_0. \tag{2.19}$$

The matrix $A_{\mathrm{f}i}$ must be made Hurwitz for all $i\in\mathcal{N}$ based on (Theorem 2, [15]). Therefore, we can obtain a unique positive-definite matrix solution $P_i\in\mathbb{R}^{(n_i+l)\times(n_i+l)}$ to the Lyapunov equation $A_{\mathrm{f}i}^{\mathrm{T}}P_i+P_iA_{\mathrm{f}i}=-Q_i$ for every given positive-definite matrix $Q_i\in\mathbb{R}^{(n_i+l)\times(n_i+l)}$. We now define $\tilde{\xi}_i(t)\triangleq\big[(x_i(t)-x_{\mathrm{r}i}(t))^{\mathrm{T}},(z_i(t)-z_{\mathrm{r}i}(t))^{\mathrm{T}}\big]^{\mathrm{T}}$ and provide an estimate of the unknown time-varying weight matrix $W_i(t)$ with the weight update law satisfying

$$\dot{\hat{W}}_i(t)=\mathrm{Proj}_{\mathrm{m}}(\hat{W}_i(t),\Gamma_{W_i}\sigma_i(x_i(t))\tilde{\xi}_i^{\mathrm{T}}(t)P_i\bar{B}_i),\quad \hat{W}_i(t_0)=\hat{W}_{i0},\quad t\geq t_0. \tag{2.20}$$

Here, $\Gamma_{W_i}\in\mathbb{R}^{s_i\times s_i}$ denotes adaptive gain matrix, which is positive-definite. From [24], [15], the uniform boundedness of the adaptive gain matrix column-wise is guaranteed by the projection operator.

Remark 3 (Uniform Ultimate Boundedness of $\tilde{y}_i(t)$) (**Theorem 3,** [15]). If we follow (2.3) and (2.4) with Assumptions 1 and 2 for all $i\in\mathcal{N}$, reference models of these agents given in (2.6), (2.7), and (2.8) that satisfy Remarks 1 and 2, the control law shown in (2.17), and the weight update law as given in

Table 2.1: The summary of the distributed adaptive control law.

Open-loop plant	$\dot{x}_i(t) = A_i x_i(t) + B_i[u_i(t) + \Delta_i(t, x_i(t))] + \delta_i(t)$ $y_i(t) = C_i x_i(t)$
Reference model	$\dot{x}_{\mathrm{r}i}(t) = A_{\mathrm{m}i} x_{\mathrm{r}i}(t) + B_{\mathrm{m}i} z_{\mathrm{r}i}(t)$ $\dot{z}_{\mathrm{r}i}(t) = \frac{1}{d_i + k_i}\left[\sum_{j \in N_i} a_{ij}\left(y_{\mathrm{r}i}(t) - y_{\mathrm{r}j}(t)\right) + k_i\left(y_{\mathrm{r}i}(t) - y_0(t)\right)\right]$ $y_{\mathrm{r}i}(t) = C_i x_{\mathrm{r}i}(t)$
Control law	$u_i(t) = -K_{1i} x_i(t) - K_{2i} z_i(t) - \hat{W}_i^{\mathrm{T}}(t)\sigma_i(x_i(t))$
Distributed integrator	$\dot{z}_i(t) = \frac{1}{d_i + k_i}\left[\sum_{j \in N_i} a_{ij}\left(y_i(t) - y_{\mathrm{r}j}(t)\right) + k_i\left(y_i(t) - y_0(t)\right)\right]$
Weight update law	$\dot{\hat{W}}_i(t) = \mathrm{Proj}_{\mathrm{m}}(\hat{W}_i(t), \Gamma_{W_i}\sigma_i(x_i(t))\tilde{\xi}_i^{\mathrm{T}}(t) P_i \bar{B}_i)$
Lyapunov equation	$A_{\mathrm{f}i}^{\mathrm{T}} P_i + P_i A_{\mathrm{f}i} = -Q_i$

(2.20), the uniform ultimate boundedness of $\tilde{y}_i(t)$ can be shown. Furthermore, if the unknown weight matrix is constant when the basis function has a bias term and unmatched external disturbances do not exist for all $i \in \mathcal{N}$, then $\lim_{t\to\infty} \tilde{y}_i(t) = 0,\ \forall i \in \mathcal{N}$.

As noted in [15], we also highlight the following. The output tracking error $e_i(t) = \tilde{y}_i(t) + e_{\mathrm{r}i}(t)$ is uniformly ultimately bounded since $e_{\mathrm{r}i}(t)$ and $\tilde{y}_i(t)$ are both uniformly ultimately bounded. In addition, if the basis function has a bias term when the unknown weight matrix is constant, unmatched external disturbances do not exist for each agent i in $\mathcal{G}$ and $\lim_{t\to\infty} \dot{y}_0(t) = 0$, then $\lim_{t\to\infty} e_i(t) = 0,\ \forall i \in \mathcal{N}$. Finally, the summary of the distributed adaptive control law overviewed above is given in Table 2.1.

2.5 Experimental Setup

The experimental setup, which we apply the proposed distributed control algorithm overviewed in Section 2.4 is shown in Figure 2.1. The setup is comprised of two cart-inverted pendulums and a cart, a track (102 [cm]), a Q8-USB data acquisition board (i.e., digital to analog converter), and two amplifiers, which are VoltPAQ-X1 and VoltPAQ-X2. Each cart is equipped with a DC motor, which enables carts to move only in x direction. In addition to the movement of the cart in horizontal direction, pendulums are able to rotate 360 [deg] in x-y plane. The desired position of the cart and the stability of pendulums are provided by the motors. From sensing point of view, each cart can access the angle of pendulum as well

as the position of the cart with the help of sensors (encoders), which are placed on each cart. The angular velocity of pendulums and the velocity of carts are calculated by derivative filters, which are provided by the manufacturer, Quanser, of this setup [1]. In addition, initial positions of each cart and initial angle of each pendulum are determined by sensors as zero at the beginning of the experiment. The controller of each agent becomes activated when the pendulum of the cart is raised to the upright position. If the cart does not have a pendulum, then it is activated manually.

A schematic of the experimental setup is shown in Figure 2.2, where the cart-inverted pendulum on the left denotes the first agent, the cart in the middle denotes the second agent, and the cart-inverted pendulum on the right denotes the third agent. We consider that these agents communicate each other and exchange the information required by the distributed adaptive control architecture with respect to the graph topology shown in Figure 2.3, which clearly satisfies Assumption 4. Agents are experimentally expected to not only follow the output of the leader but also stabilize the pendulums as long as they have pendulums.

We first begin by presenting the equations of motion of this experimental setup. Since the first and the third agents have pendulums, they have 4 state variables, which are the position and the velocity of the cart as well as the angle and the angular velocity of the pendulum. Moreover, the second agent has only the position and the velocity of the cart. Base dynamical models, notations, and parameters of the system are obtained from the user manual of the manufacturer. Finally, the linearized dynamical model for each agent

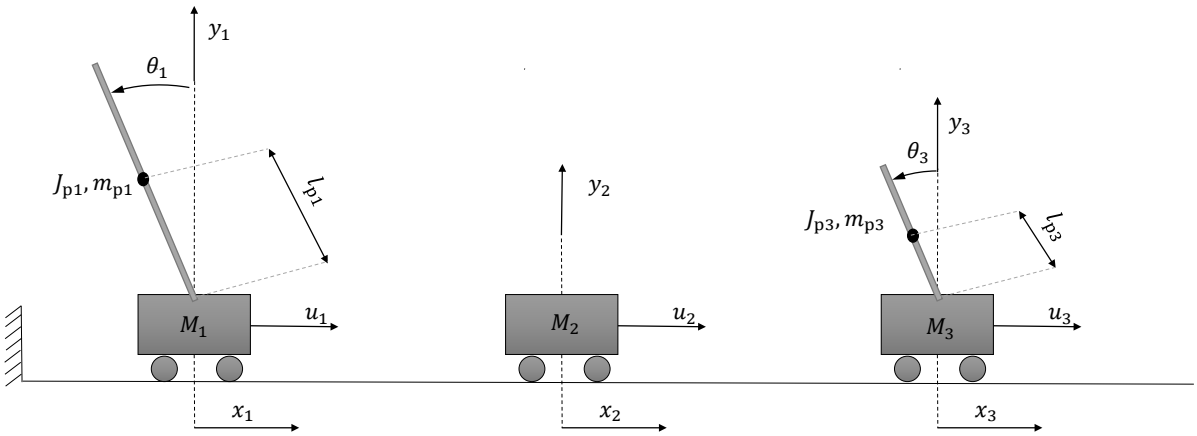

Figure 2.2: Schematic of the experimental setup.

is represented in the form given by

$$\dot{x}_i(t) = A_i x_i(t) + B_i u_i(t), \quad x_i(0) = x_{i0}, \quad t \geq 0, \tag{2.21}$$

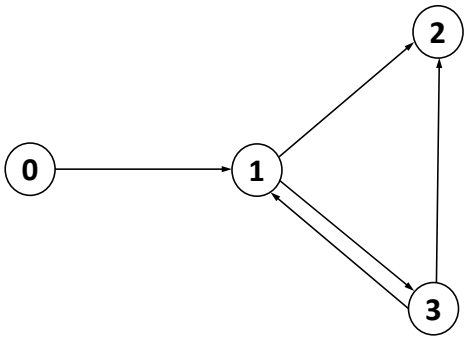

Figure 2.3: Graph topology between agents and the leader.

where

$$\begin{bmatrix} \dot{x}_1(t) \\ \dot{\theta}_1(t) \\ \ddot{x}_1(t) \\ \ddot{\theta}_1(t) \end{bmatrix} = \underbrace{\begin{bmatrix} 0 & 0 & 1 & 0 \\ 0 & 0 & 0 & 1 \\ 0 & \frac{m_{p1}^2 l_{p1}^2 g}{J_{t1}} & \frac{-(J_{p1}+m_{p1}l_{p1}^2)(r_{mp}^2 R_m B_{eq}+K_m\tau_g K_g^2\tau_m K_t)}{r_{mp}^2 R_m J_{t1}} & \frac{-m_{p1}l_{p1}B_{p1}}{J_{t1}} \\ 0 & \frac{(J_{eq1}+m_{p1})l_{p1}m_{p1}g}{J_{t1}} & \frac{-(m_{p1}l_{p1})(r_{mp}^2 R_m B_{eq}+K_m\tau_g K_g^2\tau_m K_t)}{r_{mp}^2 R_m J_{t1}} & \frac{-(J_{eq1}+m_{p1})B_{p1}}{J_{t1}} \end{bmatrix}}_{A_1} \begin{bmatrix} x_1(t) \\ \theta_1(t) \\ \dot{x}_1(t) \\ \dot{\theta}_1(t) \end{bmatrix}$$

$$+ \underbrace{\begin{bmatrix} 0 \\ 0 \\ \frac{(J_{p1}+m_{p1}l_{p1}^2)\tau_g K_g \tau_m K_t}{r_{mp}R_m J_{t1}} \\ \frac{(m_{p1}l_{p1})\tau_g K_g \tau_m K_t}{r_{mp}R_m J_{t1}} \end{bmatrix}}_{B_1} u_1(t), \qquad y_1 = \underbrace{\begin{bmatrix} 1 & 0 & 0 & 0 \end{bmatrix}}_{C_1} \begin{bmatrix} x_1(t) \\ \theta_1(t) \\ \dot{x}_1(t) \\ \dot{\theta}_1(t) \end{bmatrix} \tag{2.22}$$

$$\begin{bmatrix} \dot{x}_2(t) \\ \ddot{x}_2(t) \end{bmatrix} = \underbrace{\begin{bmatrix} 0 & 1 \\ 0 & \frac{-(B_{eq}R_m r_{mp}^2+\tau_g K_g^2 K_m \tau_m K_t)}{R_m r_{mp}^2 J_{eq2}} \end{bmatrix}}_{A_2} \begin{bmatrix} x_2(t) \\ \dot{x}_2(t) \end{bmatrix} + \underbrace{\begin{bmatrix} 0 \\ \frac{\tau_g K_g \tau_m K_t}{R_m r_{mp} J_{eq2}} \end{bmatrix}}_{B_2} u_2(t), \qquad y_2 = \underbrace{\begin{bmatrix} 1 & 0 \end{bmatrix}}_{C_2} \begin{bmatrix} x_2(t) \\ \dot{x}_2(t) \end{bmatrix} \tag{2.23}$$

$$\begin{bmatrix} \dot{x}_3(t) \\ \dot{\theta}_3(t) \\ \ddot{x}_3(t) \\ \ddot{\theta}_3(t) \end{bmatrix} = \underbrace{\begin{bmatrix} 0 & 0 & 1 & 0 \\ 0 & 0 & 0 & 1 \\ 0 & \frac{m_{\mathrm{p3}}^2 l_{\mathrm{p3}}^2 g}{J_{\mathrm{t3}}} & \frac{-(J_{\mathrm{p3}}+m_{\mathrm{p3}} l_{\mathrm{p3}}^2)(r_{\mathrm{mp}}^2 R_{\mathrm{m}} B_{\mathrm{eq}}+K_{\mathrm{m}}\tau_{\mathrm{g}} K_{\mathrm{g}}^2 \tau_{\mathrm{m}} K_{\mathrm{t}})}{r_{\mathrm{mp}}^2 R_{\mathrm{m}} J_{\mathrm{t3}}} & \frac{-m_{\mathrm{p3}} l_{\mathrm{p3}} B_{\mathrm{p3}}}{J_{\mathrm{t3}}} \\ 0 & \frac{(J_{\mathrm{eq3}}+m_{\mathrm{p3}}) l_{\mathrm{p3}} m_{\mathrm{p3}} g}{J_{\mathrm{t3}}} & \frac{-(m_{\mathrm{p3}} l_{\mathrm{p3}})(r_{\mathrm{mp}}^2 R_{\mathrm{m}} B_{\mathrm{eq}}+K_{\mathrm{m}}\tau_{\mathrm{g}} K_{\mathrm{g}}^2 \tau_{\mathrm{m}} K_{\mathrm{t}})}{r_{\mathrm{mp}}^2 R_{\mathrm{m}} J_{\mathrm{t3}}} & \frac{-(J_{\mathrm{eq3}}+m_{\mathrm{p3}}) B_{\mathrm{p3}}}{J_{\mathrm{t3}}} \end{bmatrix}}_{A_3} \begin{bmatrix} x_3(t) \\ \theta_3(t) \\ \dot{x}_3(t) \\ \dot{\theta}_3(t) \end{bmatrix}$$

$$+ \underbrace{\begin{bmatrix} 0 \\ 0 \\ \frac{(J_{\mathrm{p3}}+m_{\mathrm{p3}} l_{\mathrm{p3}}^2)\tau_{\mathrm{g}} K_{\mathrm{g}} \tau_{\mathrm{m}} K_{\mathrm{t}}}{r_{\mathrm{mp}} R_{\mathrm{m}} J_{\mathrm{t3}}} \\ \frac{(m_{\mathrm{p3}} l_{\mathrm{p3}})\tau_{\mathrm{g}} K_{\mathrm{g}} \tau_{\mathrm{m}} K_{\mathrm{t}}}{r_{\mathrm{mp}} R_{\mathrm{m}} J_{\mathrm{t3}}} \end{bmatrix}}_{B_3} u_1(t), \qquad y_3 = \underbrace{\begin{bmatrix} 1 & 0 & 0 & 0 \end{bmatrix}}_{C_3} \begin{bmatrix} x_3(t) \\ \theta_3(t) \\ \dot{x}_3(t) \\ \dot{\theta}_3(t) \end{bmatrix} \tag{2.24}$$

with $J_{\mathrm{eq}i} = M_i + \frac{\tau_{\mathrm{g}} K_{\mathrm{g}}^2 J_{\mathrm{m}}}{r_{\mathrm{mp}}^2}$ and $J_{\mathrm{t}i} = J_{\mathrm{eq}i} J_{\mathrm{p}i} + J_{\mathrm{eq}i} m_{\mathrm{p}i} l_{\mathrm{p}i}^2 + m_{\mathrm{p}i} J_{\mathrm{p}i}$. The variable $u_i(t)$ denotes the voltage, which is given into the cart as a control input. The variable $x_i(t)$ and $\theta_i(t)$ denote the position of the cart and the angle of the pendulum, respectively. All the parameters in the experimental setup highlighted above are shown in Tables 2.2 and 2.3. After inserting all numerical values of the parameters in the experimental setup into (2.22), (2.23), and (2.24), we obtain A_i, B_i, and C_i matrices for all $i \in \mathcal{N}$. These A_i, B_i, and C_i matrices for each agent satisfy Assumptions 6 and 7.

Table 2.2: Notations used in dynamical modeling.

τ_{m}	Motor Efficiency	$J_{\mathrm{p}i}$	Pendulum Inertia
τ_{g}	Planetary Gearbox Efficiency	$m_{\mathrm{p}i}$	Mass of Pendulum with T fitting
K_{g}	Planetary Gearbox Gear Ratio	M_i	Mass of Cart
K_{t}	Motor Current Torque Constant	B_{eq}, $B_{\mathrm{p}i}$	Equivalent Viscous Damping Coefficient at the cart and at the pendulum
K_{m}	Motor Back-emf Constant	$l_{\mathrm{p}i}$	Pendulum Length
R_{m}	Motor Armature Resistance	r_{mp}	Motor Pinion Radius
g	Gravitational Constant on Earth	J_{m}	Rotor Moment of Inertia

Table 2.3: System parameters [1].

τ_{m}	1	J_{p1}, J_{p3}	7.88×10^{-3}, 1.20×10^{-3} kgm^2
τ_{g}	1	m_{p1}, m_{p3}	0.23, 0.127 kg
K_{g}	3.71	M_1=M_2=M_3	0.507 kg
K_{t}	7.68×10^{-3} Nm/A	B_{eq}, B_{p1}=B_{p3}	4.3, 0.0024 Nms/rad
K_{m}	7.68×10^{-3} V/(rad/s)	l_{p1}, l_{p3}	0.6413, 0.3365 m
R_{m}	2.6 Ω	r_{mp}	6.35×10^{-3}m
g	9.79 m/s^2	J_{m}	3.9×10^{-7}kgm^2

2.6 Experimental Results

In this section, we present the experimental results on the multiagent mechanical platform shown in Figure 2.1 in order to demostrate the efficacy of the proposed distributed adaptive architecture. In particular, we present the steps we take to design the proposed distributed adaptive controller for each agent. Then, we compare the following two cases:

(i) The adaptive augmentation is off (i.e., $u_i(t) = u_{\mathrm{n}i}(t)$).

(ii) The adaptive augmentation is on (i.e., $u_i(t) = u_{\mathrm{n}i}(t) - u_{\mathrm{ad}i}(t)$ as in (2.17)).

In our mechanical experimental platform shown in Figure 2.1, the main source of uncertainty is due to the friction. As it is known, system uncertainties can degrade the performance of physical systems. For instance, using a simple model of viscous friction (kinetic friction) or underestimating the size of a friction coefficent in the modeling of an inverted pendulum system can result in oscillative or even unstable system responses [28]. In our system, kinetic and static frictions are treated as unknown. In addition to the friction, it is also observed while conducting the experiment that the cables connecting carts to the amplifiers and the digital analog converter may impact the system performance; hence, they represent other uncertainty sources.

In what follows, we first obtain the parameters of nominal controller for each agent through a linear quadratic regulator-based design with solving the associated algebraic Riccati equation. These parameters (i.e., K_{1i} and K_{2i}) are listed in Table 2.4. They guarantee that $A_{\mathrm{f}i}$ is Hurwitz and the agent-wise local sufficient condition (2.15) holds for all $i \in \mathcal{N} = \{1,2,3\}$. Now, we construct the dynamics of the reference model for each agent based on (2.6), (2.7), and (2.8). Second, the parameters of the adaptive controller for each agent are selected as follows. The term P_i in the weight update law (2.20) is obtained by selecting Q_i in the Lyapunov equation as an identity matrix for $i = 1,2,3$. The basis function in the weight update law of each agent has a bias term and is written in a compact form in Table 2.4. The adaptive gain matrix Γ_{W_i}, the projection tolerance ε_θ, and the projection norm bound $W_{\max i}$ of each agent are listed in Table 2.4. Finally, we select the value of Γ in projection operators of each agent as being equal to Γ_{W_i}.

Let the unknown dynamics of the leader be given by

$$\dot{y}_0(t) = -y_0(t) + c(t), \tag{2.25}$$

which satisfies Assumption 3, where

Table 2.4: Experimental parameters.

K_{11}, K_{21}	$[-61.7064, 137.1485, -47.1679, 25.3439]$, $[-20]$	Γ_{W_1}	diag $(420, 350, 350, 350, 350)$
K_{12}, K_{22}	$[323.5980, 18.6588]$, $[141.4214]$	Γ_{W_2}	diag $(5, 5, 5)$
K_{13}, K_{23}	$[-35.5580, 61.6055, -27.9752, 8.7089]$, $[-12.2474]$	Γ_{W_3}	diag $(448, 336, 224, 168, 28)$
$\sigma_i(.)$ for $i = 1, 3$	$[1, x_i, \theta_i, \dot{x}_i, \dot{\theta}_i]^{\mathrm{T}}$	$W_{\max 1} = W_{\max 2} = W_{\max 3}$	2
$\sigma_i(.)$ for $i = 2$	$[1, x_i, \dot{x}_i]^{\mathrm{T}}$	ε_θ	0.01

$$c(t) = \begin{cases} 10 & \text{if } 10+70k > t \geq 10+70(k-1), \text{ where } k\text{=1,3,5,7,} \\ \text{-10} & \text{if } 10+70k > t \geq 10+70(k-1), \text{ where } k\text{=2,4,6.} \end{cases}$$

Note that the first 10 seconds are not given here since the experimental plots associated with that time interval are only related to system initialization. Moreover, since our experimental setup consists of three agents, instantaneously activating the adaptive controller of each agent manually during the experiment is not trivial; hence, this activation time interval is showed in the shaded areas of all the following figures.

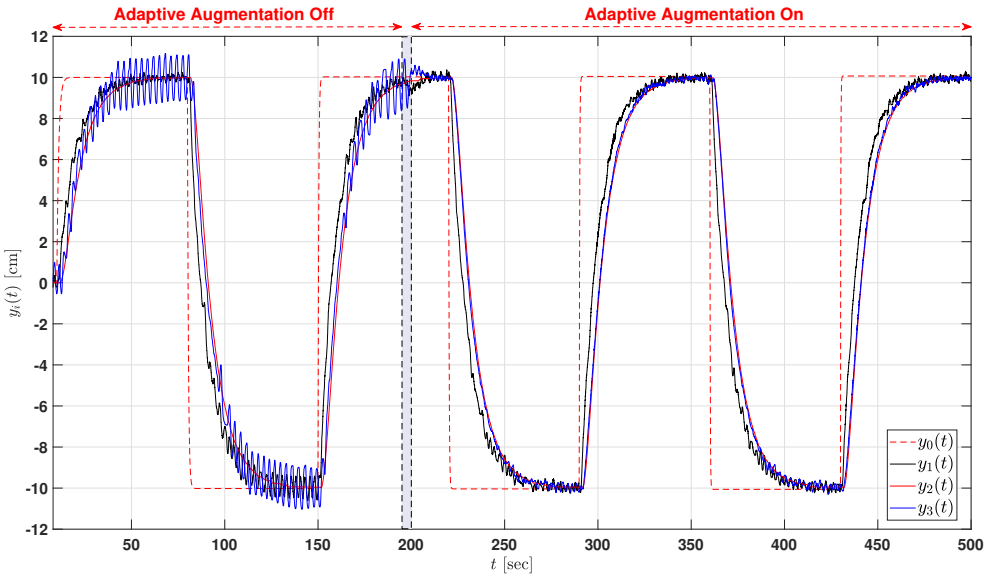

Figure 2.4: Tracking performances of each agent without and with the adaptive augmentation.

Figure 2.4 shows the trajectory of the leader and the tracking performances of each agent without and with the adaptive augmentation. When the adaptive augmentation is off, agents track the output of the leader with large amplitude of oscillations primarily due to the effect of the friction. After activating the adaptive controller, the amplitude of oscillations are substantially decreased as it is seen in Figure 2.4. In Figures 2.5,

2.6, and 2.7, the trajectories of the reference model of each agent in conjunction with the outputs of each agent without and with the adaptive augmentation are shown for $i = 1, 2, 3$. It is clear that the third agent with the adaptive controller shows the most significant improvement in terms of decreasing the amplitude of oscillations among all agents. Note also that the response of the second agent without and with the adaptive augmentation is nearly indistinguishable. Figure 2.8 shows the deviations of the first and the third pendulums from the desired angle, which is zero degree, without and with the adaptive augmentation. One important feature in Figure 2.8 is that the improvement in terms of decreasing the amplitude of the deviations of the pendulums from the desired angle is consistent with the improvement in the outputs of the first and the third agents (the output tracking error) in Figures 2.5 and 2.7.

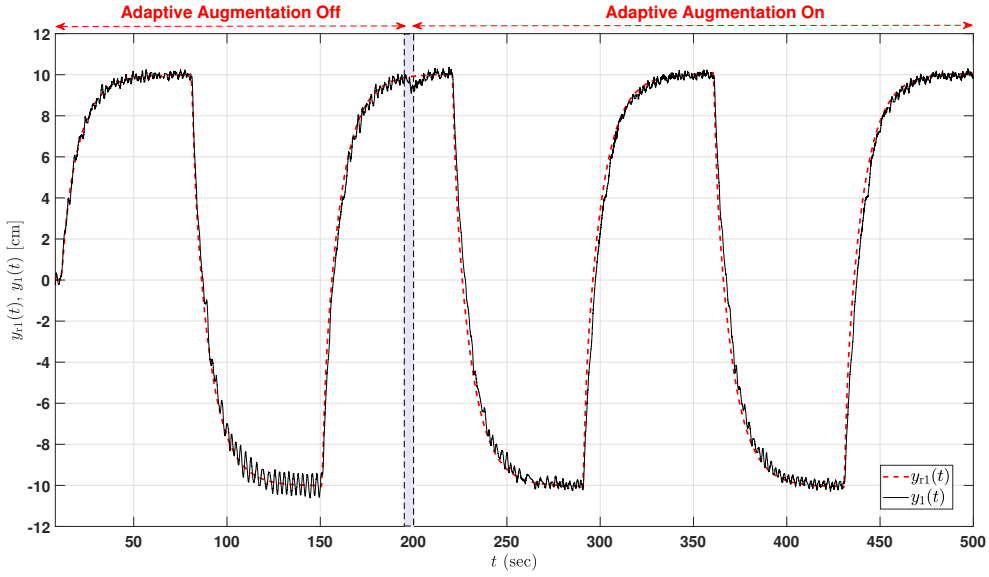

Figure 2.5: The reference model tracking performance of the first agent without and with the adaptive augmentation.

We can see the applied control inputs into the agents in Figure 2.9 corresponding to the results in Figures 2.4, 2.5, 2.6, 2.7, and 2.8. It is apparent from Figure 2.9 that a slight increase is seen on the amplitude of the voltage (control input) applied to the first agent after activating the adaptive controller. On the other hand, the frequency of the voltage implemented to the third agent increases after turning on the adaptive controller. The Euclidean norm of the estimated weight of each agent is shown in Figure 2.10. Since the norm of the estimated weight of the second agent is so small, it is seen like a line on the horizontal axis of

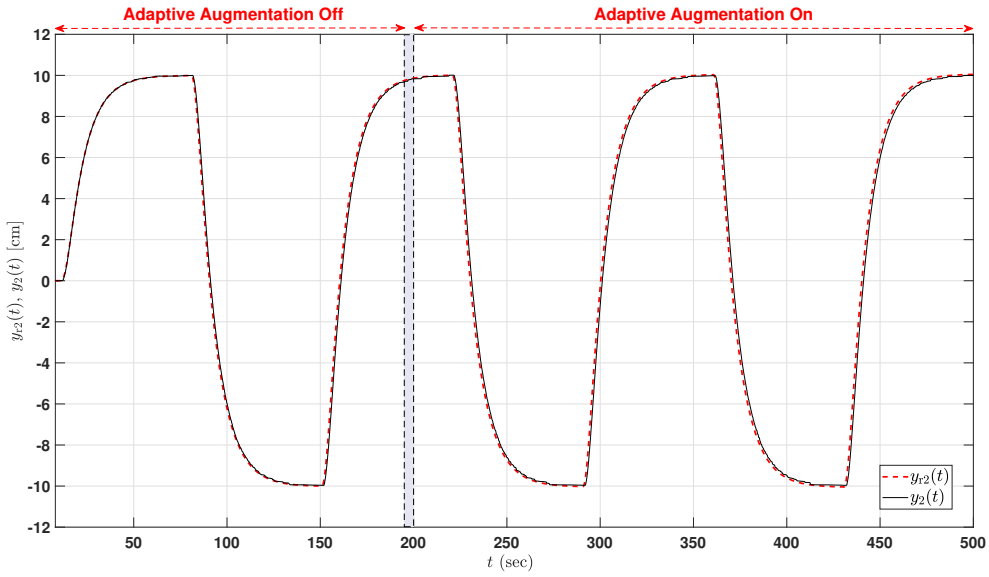

Figure 2.6: The reference model tracking performance of the second agent without and with the adaptive augmentation.

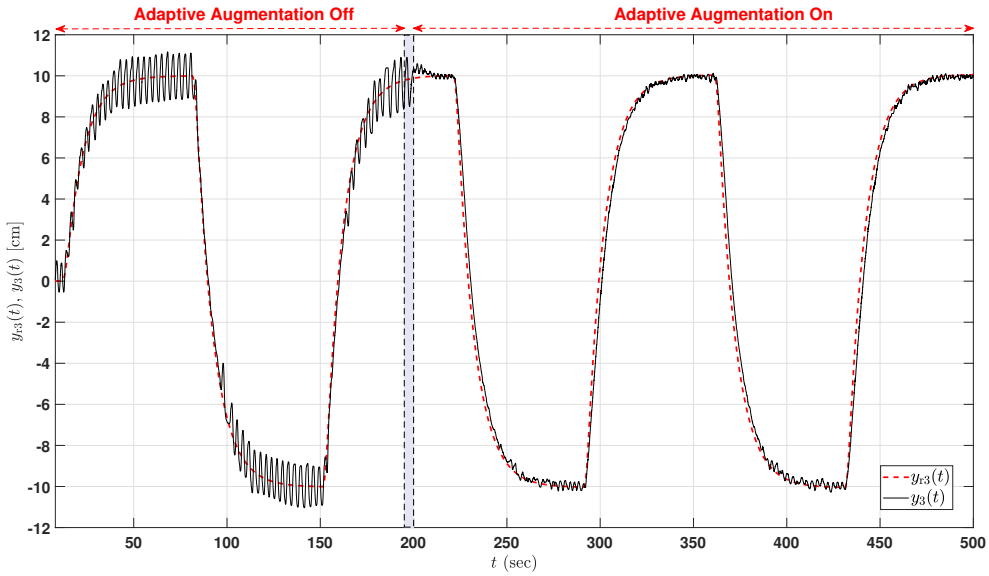

Figure 2.7: The reference model tracking performance of the third agent without and with the adaptive augmentation.

the second plot. On the other hand, the norms of the estimated weight of the first and the third agents hit their projection norm bounds $W_{\max 1}$ and $W_{\max 3}$ during the experiment.

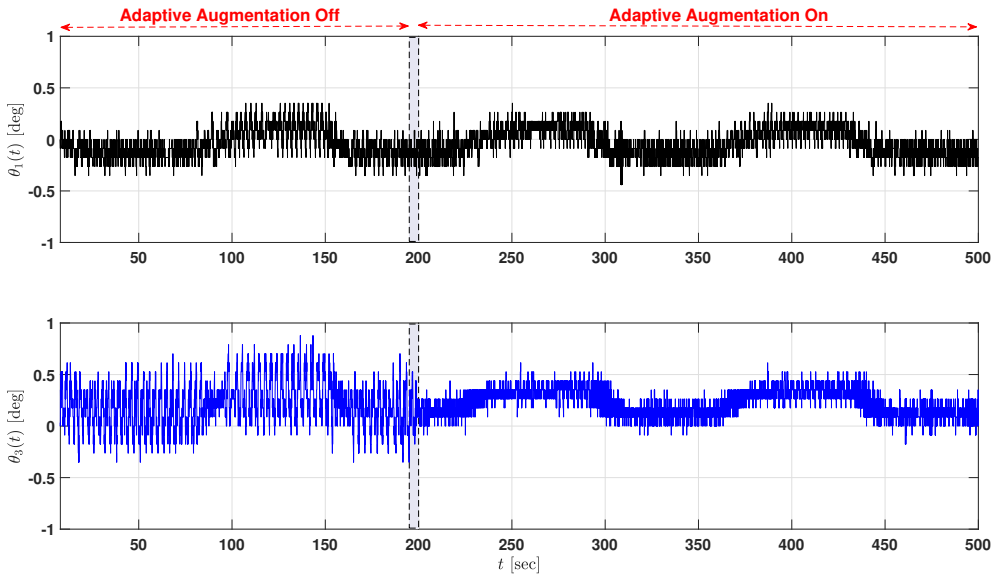

Figure 2.8: Angle of the pendulums of the first and the third agents without and with the adaptive augmentation.

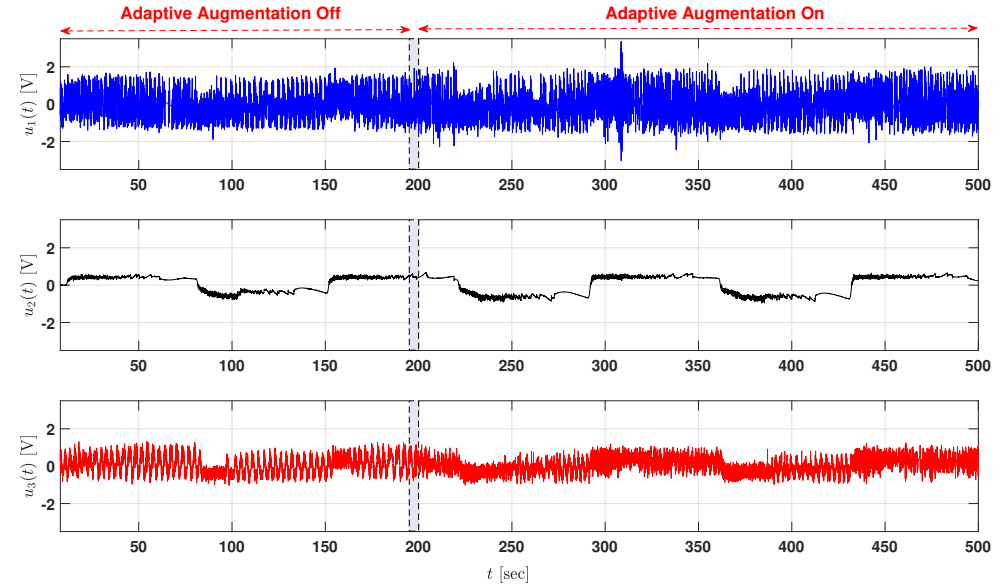

Figure 2.9: Applied control inputs to each agent without and with the adaptive augmentation.

2.7 Conclusions

This paper presented experimental evaluation of a recently proposed distributed adaptive controller approach [15] on a heterogeneous multiagent mechanical platform. Experiments revealed that the adaptive augmentation of the controller suppressed the effect of the uncertainties and disturbances effectively. In

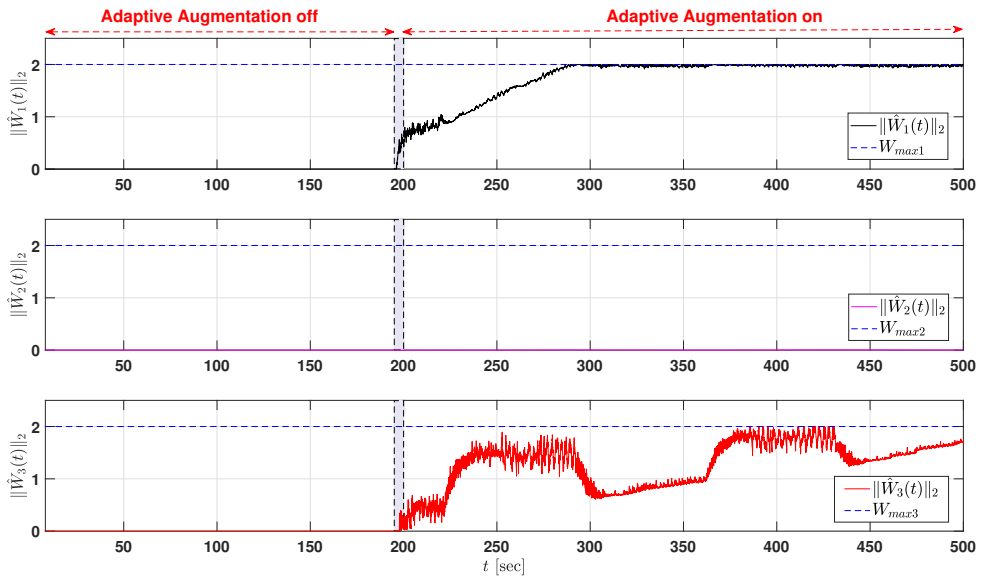

Figure 2.10: The Euclidean norm of the estimated weight of each agent.

particular, the tracking results with the adaptive augmentation outperforms the ones with the nominal controller. Future research can include experimentation on a group of mobile robots evolving in two- and three-dimensional spaces.

2.8 Acknowledgments

The authors would like to thank K. M. Dogan for her helpful responses to our questions regarding the experimental setup. This research was supported by the Dynamics, Control, and Systems Diagnostics Program of the National Science Foundation under Grant CMMI-1657637.

CHAPTER 3: CONTROLLING THE MULTIAGENT SYSTEM WITH LIMITED RESOURCES IN THE PRESENCE OF A MISBEHAVING AGENT

In this paper, we focus on multiagent systems that involve agents executing local information exchange predicated on the Laplacian matrix. For this class of systems, it is known that a small perturbation may result in unstable behavior due to their nominal stability properties. In particular, unlike the existing results proposing controllers for each agent separately to robustify the overall closed-loop multiagent system subject to a disturbance, we investigate the case in which a limited number of control inputs can be applied to the agents (i.e., driver agents) in the system under the disturbance (we specifically focus on only one control input). To this end, we first show that the trajectories of all agents in the multiagent system with a fixed, connected, and undirected graph, where the system subject to a bounded disturbance through an agent, remain bounded with only one control input having a bounded command regardless of which agent we apply the control input. The steady-state values of these agents are then derived when the control input is applied to an undisturbed agent and a disturbed (i.e., misbehaving) agent, respectively. Finally, we propose a graph-theoretical approach for multiagent systems having a fixed, connected, and undirected acyclic graph that gives the steady-state values of all agents. This approach provides a way to show that the largest steady-state deviation from the desired command in the multiagent system is minimized if the driver agent is located as close as possible to the misbehaving agent. Several numerical examples are also presented to illustrate the implementation of our theoretical results.

3.1 Introduction

Multiagent systems consist of groups of agents, which process the distributed information and work cooperatively through a graph topology. Distributed control of these systems has been an active research topic in the recent decades owing to their broad applications such as mobile robots and unmanned aerial vehicles (e.g., see [29], [23], [30] and references therein). Technological developments in networking and producing electromechanical systems in a miniature scale pave the way for controlling large scale systems

with the distributed control law. The use of distributed control provides the scalability and flexibility to these large scale multiagent systems. However, the lack of monitoring and controlling each agent from the central authority makes the multiagent system using distributed control susceptible to cyber-attacks and malfunctions [16]. In the literature, there has been ample studies for scenarios, where the system is subject to a disturbance and each agent is equipped with advanced controllers in addition to neighbor-based controllers (e.g., see [31], [32], [33], and [17]). Then, a natural question that arises is how to control a large scale multiagent system composed of agents having neighbor-based local controllers without implementing as many advanced controllers (i.e., limited resources) as previous studies if the system is subject to a disturbance (i.e. a cyber-attack or malfunction).

Our problem is motivated by many applications. In particular, sensor networks are a great example for large scale systems, which are prone to have malfunctioning sensors. Sensor networks are composed of a huge number of low-cost, wireless and small battery-powered sensors that are densely placed in order to take a measurement of their environment and relay the data to a central processor (fusion center) by wireless links. Since these low-cost sensors have the small size and are subject to energy constraints, their capabilities in terms of signal processing, data transmission, and storing data are limited. Due to undesired environmental effect and hardware or software failures, some sensors may stop functioning or may work improperly and relay false data in the network [19]. When a sensor starts to malfunction, it (misbehaving agent) provides false value to its sensor neighbors and this results in dragging the whole system towards the faulty sensor value [20].

To support the motivation, we give the second example. The use of multiple unmanned vehicles instead of a single vehicle for large scale operations is more advantageous in terms of addressing given missions faster in time. Every member of the group of unmmanned vehicles has a common goal and works collectively to achive that mission objective. A group of unmanned vehicles is used for various large scale important cooperative missions such as exploration of landmine fields [34], forest-fire surveillance [35], and border patrol [36]. Due to hazardous environment and dangerous activities, these low-cost unmanned vehicles in the multiagent system may stop working or may not work properly [37]. This cause a bias effect to the whole multiagent system similar to the sensor networks and pull the network to undesired point.

Lastly, other examples come from power systems and biology, respectively. Due to high cost of fossil fuels and environmental challenges, distibuted generators have been emerging among power industry. Even though a distributed generator produces considerable less energy comparing to a fossil fuel power

plant, a cluster of these generators deliver sufficient electric energy to domestic customers. However, these systems are vulnerable to cyber-attacks and communication failures [38], [39]. Human brain is a large complex system composed of a great number of neurons connected to each other, which form of a specialized clusters. The advancement of neuroimaging technology paved the way for obtaining full information about the human connectome and identify the changes related to brain diseases such as Parkinson's disease, Schizophrenia, and epilepsy. Due to these diseases, some brain regions function improperly (malfunctioning) and these parts of the human brain propagate the effect of the disease by relaying disordered information (false data) to healthy brain regions via neural connections. This results in continuing anatomical network disruption [40] - [42].

The contribution of this paper is to address the problem stated in the first paragraph. We first show that a multiagent system composed of agents only processing the distributed information based on the Laplacian matrix shows unstable behavior with a small perturbation. Then, we propose a proportional integral controller for a driver agent to make the resulting closed-loop system matrix of the multiagent system Hurwitz. After that, we introduce two methods to derive the steady-state value of each agent in the multiagent system whose graph topology for the first method is fixed, connected and undirected and for the second method is a fixed, connected, and undirected acyclic graph. While the second method is applicable to only the acyclic graph, it does not require an inverse of a matrix dependent on the graph topology. Additionally, the second method demonstrates that the largest steady-state deviation from the desired command in the multiagent system is minimized if the driver agent is located as close as possible to the misbehaving agent.

This paper is organized as follows. In Section 3.2, we introduce the mathematical and graph-theoretical notations. In Section 3.3, we formulate the problem based on the question in the introduction and present the stability analysis of the multiagent system in the presence of a disturbance without an agent, where the control input is applied. We then show that the resulting closed-loop system matrix of the multiagent system is Hurwitz with a control input and the steady-state value of the multiagent system subject to a disturbance with an agent, where the control input is applied, is obtained by using the first method in Section 3.4. In Section 3.5, we propose a second method to obtain the steady-state value of each agent in the system and also show that the largest steady-state deviation from the desired command in the multiagent system is minimized if the driver agent is located as close as possible to the misbehaving agent. Illustrative numerical examples are given in Section 3.6 to show that the theoretical results proposed in this

paper matches the values obtained from numerical examples. Finally, concluding remarks are summarized in Section 3.7.

3.2 Mathematical Preliminaries

Throughout this paper, we use the following notation. Specifically, $\mathbb{R}$ and $\mathbb{R}_{>0}$ denote the set of real and positive real numbers, respectively. Moreover, the set of $n \times 1$ real column vector is denoted by $\mathbb{R}^n$, the set of $n \times 1$ real column vector of all ones is denoted by $\mathbf{1}_n$, the set of $n \times m$ matrix is denoted by $\mathbb{R}^{n\times m}$, and the $n \times n$ identity matrix is denoted by I_n. Furthermore, $(\cdot)^{\mathrm{T}}$ denotes the transpose of a matrix, $(\cdot)^{-1}$ denotes the inverse of a nonsingular matrix, $|x|$ denotes the absolute value of a real number x, and $\triangleq$ denotes equality by definition. Finally, $\mathrm{diag}(a_1,..,a_n)$ denotes a diagonal matrix with scalar entries $a_1,...,a_n$ on its diagonal.

We now present the graph-theoretical notation and facts used in this paper, which is based on [29] and [43]. A nonempty, fixed (i.e., time-invariant), and undirected graph $\mathcal{G}$ is defined as the pair $\mathcal{G} = (V,E)$, where $V = \{v_1,\ldots,v_n\}$ is a nonempty finite set of n nodes (or vertices) and $E \subseteq [V]^2$ is a set of edges (i.e., the elements of E are 2-element subsets of V). The number of vertices of $\mathcal{G}$ is its order, written as $|\mathcal{G}|$. The union of two graphs $\mathcal{G}$ and $\mathcal{G}' = (V',E')$ is defined as $\mathcal{G} \cup \mathcal{G}' = (V \cup V', E \cup E')$. We refer to vertices and edges of $\mathcal{G}$ as $V(\mathcal{G})$ and $E(\mathcal{G})$, respectively, and an edge $\{v_i,v_j\}$ is written as e_{ij} (or e_{ji}). Two vertices v_i, v_j of $\mathcal{G}$ are adjacent (or neighbors) if $e_{ij} \in E(\mathcal{G})$. The set of neighbors of a vertex v_i is denoted by $N(v_i)$ and defined by $N(v_i) = \{v_j \in V(\mathcal{G}) : e_{ij} \in E(\mathcal{G})\}$. A path P of length r from v_l to v_j (or between v_l and v_j) in $\mathcal{G}$ is a sequence of $r+1$ distinct vertices starting with v_l (or v_j) and ending with v_j (or v_l) such that consecutive vertices are adjacent. Note that r is allowed to be zero, so a path can consist of only one vertex. In the previous definition, if $e_{jl} \in E(\mathcal{G})$ and $e_{jl} \notin E(P)$, then $P \cup e_{jl}$ is called a cycle in $\mathcal{G}$. An acyclic graph is a graph with no cycles. The distance $d_{\mathcal{G}}(v_l,v_j)$ between two vertices v_l and v_j in $\mathcal{G}$ is the length of a shortest path between v_l and v_j; if no such path exists, set $d_{\mathcal{G}}(v_l,v_j) \triangleq \infty$. The graph $\mathcal{G}$ is called connected if there exists a path between any two of its vertices. Moreover, the adjacency matrix $A(\mathcal{G}) = [a_{ij}] \in \mathbb{R}^{n\times n}$ is defined as follows: $a_{ij} = 1$ if $e_{ij} \in E(\mathcal{G})$ and $a_{ij} = 0$ otherwise. The degree and the Laplacian matrices are defined as $D(\mathcal{G}) = \mathrm{diag}(d_1,\ldots,d_N)$ with $d_i = \sum_{v_j \in N(v_i)} a_{ij}$ for all $v_i \in V(\mathcal{G})$ and $\mathcal{L}(\mathcal{G}) = D(\mathcal{G}) - A(\mathcal{G})$, respectively. By definition, $\mathcal{L}(\mathcal{G})$ has zero row sums (i.e., $\mathcal{L}(\mathcal{G})\mathbf{1}_n = 0$). It is also known that $\mathcal{L}(\mathcal{G})$ is positive semidefinite. The graph $\mathcal{G}$ is connected if, and only if, the second smallest eigenvalue of $\mathcal{L}(\mathcal{G})$ is in $\mathbb{R}_{>0}$.

3.3 Problem Formulation

In this paper, we focus on multiagent systems in the presence of a misbehaving agent. To formulate our problem, let this system be composed of n single integrator interconnected agents over a fixed, connected, and undirected graph $\mathcal{G}$, where each agent is denoted by a distinct node v_i in $\mathcal{G}$. Every agent has access to the relative state information with respect to its neighbors. Moreover, agents can be categorized into 3 groups: The driver agent, where the control input is applied, the misbehaving agent, which is subject to the disturbance, and floating agents, which are directly exposed to neither the control input nor the disturbance. Specifically, an agent can be considered the misbehaving agent and the driver agent simultaneously if the agent is exposed to both the disturbance and the control input.

Mathematically, let $x_i(t) \in \mathbb{R}$ denote the state of each agent in $\mathcal{G}$. This system can be compactly represented in the form given by

$$\dot{x}(t) = -\mathcal{L}(\mathcal{G})x(t) + bu(t) + dw(t),\ x(0) = x_0,\ t \geq 0 \tag{3.1}$$

$$y(t) = b^{\mathrm{T}}x(t), \tag{3.2}$$

where $x(t) = [x_1(t), \ldots, x_n(t)]^{\mathrm{T}} \in \mathbb{R}^n$ denotes the aggregated state vector, $u(t) \in \mathbb{R}$ denotes the control input, $w(t) \in \mathbb{R}$ denotes the disturbance, and $y(t) \in \mathbb{R}$ denotes the output (i.e., the state of the driver agent). Furthermore, $b \in \mathbb{R}^n$ determines the driver agent and $d \in \mathbb{R}^n$ determines the misbehaving agent. In particular, b is the unit vector with a 1 in the k^{th} element, where the control input is applied to only the k^{th} agent. Similarly, d is also a unit vector with a 1 in the l^{th} element, where only the l^{th} agent in the multiagent system is subject to the disturbance.

To motivate our problem, we first illustrate the case, in which a control input is not applied to the system (3.1). In this case, (3.1) reduces to

$$\dot{x}(t) = -\mathcal{L}(\mathcal{G})x(t) + dw(t), \quad x(0) = x_0, \quad t \geq 0, \tag{3.3}$$

where $w(t)$ is a piecewise continuous function of time. If the disturbance satisfies $\lim_{t\to\infty} \int_0^t w(\tau)d\tau = \pm\infty$[1], then $x(t)$ is unbounded as $t \to \infty$.

[1] We consider this in the extended real number system. Note that nonzero constant functions automatically satisfy this condition.

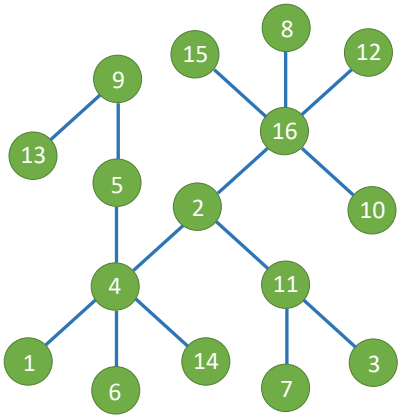

Figure 3.1: The graph topology of the multiagent system composed of 16 agents.

Consider the given system (3.3). Since $\mathcal{L}(\mathcal{G})$ is a symmetric matrix, it is orthogonally diagonalizable owing to the spectral theorem[2] in [44]. Therefore, there exists an orthogonal matrix T for $\mathcal{L}(\mathcal{G})$ such that $\mathcal{L}(\mathcal{G}) = T\Lambda T^{-1}$, where Λ is a diagonal matrix whose diagonal entries are the eigenvalues of $\mathcal{L}(\mathcal{G})$. Now, we can apply a similarity transformation to (3.3) with

$$\xi(t) \triangleq T^{-1}x(t). \tag{3.4}$$

Along with (3.3) and (3.4), we obtain

$$\dot{\xi}(t) = -\Lambda\xi(t) + T^{-1}dw(t), \quad \xi(0) = \xi_0, \quad t \geq 0, \tag{3.5}$$

where

$$\Lambda = \begin{bmatrix} \lambda_1 & & \\ & \ddots & \\ & & \lambda_n \end{bmatrix} \quad \text{and} \quad T = \begin{bmatrix} | & & | \\ v_1 & \dots & v_n \\ | & & | \end{bmatrix}.$$

By the property of the Laplacian matrix, a diagonal element λ_i in Λ matrix is zero and its corresponding right eigenvector is $\mathbf{1}_n$. Without loss of generality, we assume that λ_n is zero. By the construction of T, v_n is $\frac{1}{\sqrt{n}}\mathbf{1}_n$. By definition, $T^{-1} = T^{\mathrm{T}}$ so that n^{th} row of T^{-1} is $\frac{1}{\sqrt{n}}\mathbf{1}_n^{\mathrm{T}}$. Then n^{th} state of (3.5) can be

[2] If A is a symmetric matrix, then matrix A is orthogonally diagonalizable such that there exists an orthogonal matrix S satisfying $S^{-1}AS$, which gives a diagonal matrix whose diagonal entries are the eigenvalues of A.

written as

$$\dot{\xi}_n(t) \quad = \quad \frac{1}{\sqrt{n}} w(t), \quad \xi_n(0) = \xi_{n0}, \quad t \geq 0, \tag{3.6}$$

where $w(t)$ satisfies $\lim_{t\to\infty} \int_0^t w(\tau)d\tau = \pm\infty$. Therefore, $\xi_n(t)$ is unbounded as $t \to \infty$, so is $\xi(t)$. In conjunction with (3.4), this implies that $x(t)$ is unbounded as $t \to \infty$.

Now, we present a numerical example to show the consistency between the simulation result and the statement given in the motivational example. Consider a multiagent system with the dynamics of (3.3). The graph topology of the system is shown in Figure 3.1. In this graph, node 16 represents the misbehaving agent and the others are floating agents. Let the disturbance be $w(t) = 1 + sin(t)$, which satisfies $\lim_{t\to\infty} \int_0^t w(\tau)d\tau = +\infty$. We set all initial points of each agent between -1 and 1. Figure 3.2 defines the color of each agent used in Figure 3.3, which depicts the trajectory of each agent in the multiagent system subject a disturbance and no control input. Observe that $x(t)$ is unbounded as $t \to \infty$.

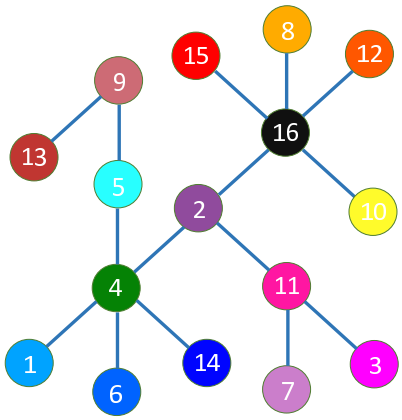

Figure 3.2: Color representation for each agent in Figure 3.3.

The purpose of this paper is to show that the trajectories of all agents in the multiagent system that consists of a misbehaving agent subject to a bounded disturbance do not diverge with only one control input having a bounded command applied to any agent in the system. In addition, we show the steady-state value of each agent in a fixed, connected, and undirected graph for two scenarios; that is; the control input is applied to a floating agent (i.e., $b \neq d$) and the misbehaving agent (i.e., $b = d$), respectively. Moreover, a graph-theoretical approach is proposed to show the steady-state value of each agent if the graph $\mathcal{G}$ is a fixed, connected and undirected acyclic graph. This approach also provides a way to show that the largest

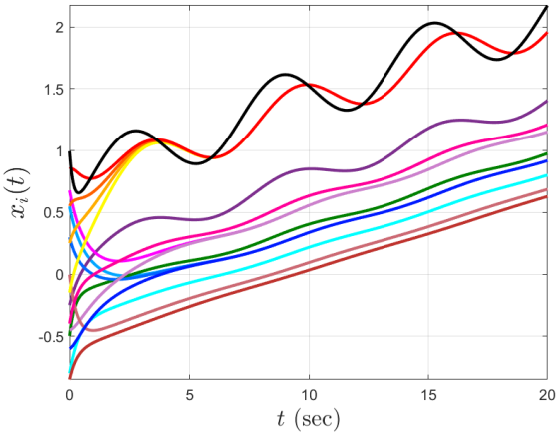

Figure 3.3: The trajectories of all agents in the multiagent system, where node 16 is subject to a disturbance and no control input is applied.

steady-state deviation from the desired command in the multiagent system is minimized if the driver agent is located as close as possible to the misbehaving agent.

3.4 Stability and Convergence Analysis

In this section, we show that the resulting closed-loop system matrix is Hurwitz regardless of which agent we implement a proportional integral controller in the multiagent system. In addition, the steady-state value of each agent is derived when the control input is applied to any agent in the system except the misbehaving agent (i.e., $b \neq d$) and directly to the misbehaving agent (i.e., $b = d$), respectively. Throughout this section, we assume that $\mathcal{G}$ is a fixed, connected, and undirected graph.

Consider the system dynamics as given in (3.1) and (3.2) with

$$u(t) = -\gamma_1 e(t) - \gamma_2 z(t), \tag{3.7}$$

$$e(t) = y(t) - c(t), \tag{3.8}$$

$$\dot{z}(t) = e(t), \quad z(0) = z_0, \quad t \geq 0, \tag{3.9}$$

where γ_1, $\gamma_2 \in \mathbb{R}_{>0}$ are the controller parameters, $z(t) \in \mathbb{R}$ denotes the integrator state, $c(t) \in \mathbb{R}$ denotes the desired command, and $e(t) \in \mathbb{R}$ denotes the tracking error between the output of the system and the desired command.

Now, using (3.2), (3.7), and (3.8), we can rewrite (3.1) as

$$\dot{x}(t) = -Jx(t) - \gamma_2 bz(t) + \gamma_1 bc(t) + dw(t), \quad x(0) = x_0, \quad t \geq 0, \tag{3.10}$$

where $J = \mathcal{L}(\mathcal{G}) + \gamma_1 bb^{\mathrm{T}}$. Also, together with (3.2) and (3.8), the integrator state given in (3.9) can be rewritten as

$$\dot{z}(t) = b^{\mathrm{T}}x(t) - c(t) \quad z(0) = z_0, \quad t \geq 0. \tag{3.11}$$

Define $\eta(t) \triangleq [x^{\mathrm{T}}(t), z(t)]^{\mathrm{T}}$. Then, (3.1), (3.2), (3.7)-(3.9) can be compactly written as

$$\dot{\eta}(t) = A_{\mathrm{g}}\eta(t) + B_{\mathrm{g}}u^*(t), \quad \eta(0) = \eta_0 \quad t \geq 0, \tag{3.12}$$

where $A_{\mathrm{g}} = \begin{bmatrix} -J & -\gamma_2 b \\ b^{\mathrm{T}} & 0 \end{bmatrix}$, $B_{\mathrm{g}} = \begin{bmatrix} \gamma_1 b & d \\ -1 & 0 \end{bmatrix}$, and $u^*(t) = \begin{bmatrix} c(t) \\ w(t) \end{bmatrix}$.

Note that $\gamma_1 bb^{\mathrm{T}}$ is a matrix whose entries are all zero except a positive element on the diagonal. By Lemma 3.3 in [23], J is a positive definite matrix.

Now, we present Lemmas 1 and 2, which play an important role for one of our main results given in Theorem 1.

Lemma 1. A_{g} matrix given in (3.12) is Hurwitz.

Proof. Let $u^*(t) \equiv 0$ in (3.12). Then, it suffices to show that the origin of (3.12) is globally asymptotically stable.

Consider the following continuously differentiable Lyapunov function candidate

$$\mathcal{V}(x,z) = \frac{1}{2}x^{\mathrm{T}}x + \frac{\gamma_2}{2}z^2. \tag{3.13}$$

Note that $\mathcal{V}(0,0) = 0$, $\mathcal{V}(x,z) > 0$ for all $(x,z) \neq (0,0)$, and the candidate is radially unbounded. The time derivative of (3.13) along the trajectories (3.10) and (3.11) can be expressed as

$$\begin{aligned}\dot{\mathcal{V}}(x(t),z(t)) &= x^{\mathrm{T}}(t)\dot{x}(t)+\gamma_2 z(t)\dot{z}(t),\\ &= -x^{\mathrm{T}}(t)Jx(t)-\gamma_2 x^{\mathrm{T}}(t)bz(t)+\gamma_2 z(t)b^{\mathrm{T}}x(t),\\ &= -x^{\mathrm{T}}(t)Jx(t)\leq 0. \end{aligned} \tag{3.14}$$

Now, let $S=\{\eta(t)\in\mathbb{R}^{n+1}:\dot{\mathcal{V}}(\eta(t))=0\}$. If $\dot{\mathcal{V}}(\eta(t))=0$, then $x(t)=0$ since J is positive definite. Hence, $S=\{\eta(t)\in\mathbb{R}^{n+1}:x(t)=0\}$. Let $\eta(t)$ be a solution that belongs identically to S: $x(t)\equiv 0\Rightarrow \dot{x}(t)\equiv 0$. From (3.10), we obtain $\gamma_2 bz(t)\equiv 0$. This implies that $bz(t)\equiv 0$ since $\gamma_2\in\mathbb{R}_{>0}$. Then, $z(t)\equiv 0$. Therefore, the only solution that identically stay in S is the trivial solution $\eta(t)\equiv 0$. Thus, the origin is the globally asymtotically stable by Corollary 4.2 in [22], as desired. ■

Remark 1. Note that A_{g} is Hurwitz irrespective of which agent we apply the control input. Since A_{g} is Hurwitz, the system in (3.12) is input-to-state stable. This implies that if $u^*(t)$ is a bounded piecewise continuous function of time, then $\eta(t)$ is bounded, so is $x(t)$.

Lemma 2. $b^{\mathrm{T}}J^{-1}=\gamma_1^{-1}\mathbf{1}_n^{\mathrm{T}}$.

Proof. Let $r^{\mathrm{T}}\triangleq b^{\mathrm{T}}J^{-1}$. Since J is positive definite, J^{-1} is positive definite. Thus, we have the following system of linear equations

$$Jr=b. \tag{3.15}$$

It is easy to verify that $r=\gamma_1^{-1}\mathbf{1}_n$ is a solution of (3.15). Since J is nonsingular, $r=\gamma_1^{-1}\mathbf{1}_n$ is the unique solution of (3.15). Hence, the result follows. ■

For the next result, we assume that $u^*(t)$ is a constant function and denoted by $\bar{u}^*=[\bar{c},\bar{w}]^{\mathrm{T}}\in\mathbb{R}^2$.

Theorem 1. Consider the compact form of the system dynamics given by (3.12). Then for all $\eta_0\in\mathbb{R}^{n+1}$, $\lim_{t\to\infty}x(t)=x^\star$, where

$$x^\star=\mathbf{1}_n\bar{c}+J^{-1}(d-b)\bar{w}. \tag{3.16}$$

In particular, if the control is applied to the misbehaving agent (i.e., $b=d$), then (3.16) reduces to

$$x^\star=\mathbf{1}_n\bar{c}. \tag{3.17}$$

Proof. Define the following assistant state

$$\zeta(t) \triangleq \eta(t) + A_{\mathrm{g}}^{-1} B_{\mathrm{g}} \bar{u}^*. \tag{3.18}$$

Inserting (3.12) into the time derivative of (3.18) and using (3.18), we obtain

$$\dot{\zeta}(t) = A_{\mathrm{g}} \zeta(t), \quad \zeta(0) = \zeta_0, \quad t \geq 0. \tag{3.19}$$

Since A_{g} is Hurwitz, $\lim_{t\to\infty} \zeta(t) = 0$ for all $\zeta_0 \in \mathbb{R}^{n+1}$. From (3.18), we have

$$\lim_{t\to\infty} \eta(t) = -A_{\mathrm{g}}^{-1} B_{\mathrm{g}} \bar{u}^*, \quad \text{for all } \eta_0 \in \mathbb{R}^{n+1}, \tag{3.20}$$

which can be also shown as

$$\begin{bmatrix} x^\star \\ z^\star \end{bmatrix} = - \begin{bmatrix} M_1 & M_2 \\ M_3 & M_4 \end{bmatrix} \begin{bmatrix} \gamma_1 b & d \\ -1 & 0 \end{bmatrix} \begin{bmatrix} \bar{c} \\ \bar{w} \end{bmatrix}, \tag{3.21}$$

where $z^\star = \lim_{t\to\infty} z(t)$ and $A_{\mathrm{g}}^{-1} = \begin{bmatrix} M_1 & M_2 \\ M_3 & M_4 \end{bmatrix}$. Since J is nonsingular and $\gamma_2 b^{\mathrm{T}} J^{-1} b = \gamma_1^{-1}\gamma_2 \in \mathbb{R}_{>0}$ by Lemma 2, $M_3 = -\gamma_2^{-1}\mathbf{1}_n^{\mathrm{T}}$ and $M_4 = -\gamma_2^{-1}\gamma_1$ by Proposition 2.8.7 in [45]. From (3.21), we have

$$z^\star = \begin{bmatrix} -\gamma_1 M_3 b + M_4 & -M_3 d \end{bmatrix} \begin{bmatrix} \bar{c} \\ \bar{w} \end{bmatrix}. \tag{3.22}$$

Inserting M_3 and M_4 into (3.22) gives $z^\star = \gamma_2^{-1}\bar{w}$. Using (3.12) and (3.20), we obtain $\lim_{t\to\infty} \dot{\eta}(t) = 0$. Thus, $\lim_{t\to\infty} \dot{x}(t) = 0$. Then, (3.10) yields

$$x^\star = J^{-1}\big(-\gamma_2 b z^\star + \gamma_1 b \bar{c} + d\bar{w}\big). \tag{3.23}$$

Inserting $z^\star$ into (3.23), one can easily show that

$$x^\star = J^{-1} \begin{bmatrix} \gamma_1 b & d - b \end{bmatrix} \begin{bmatrix} \bar{c} \\ \bar{w} \end{bmatrix}. \tag{3.24}$$

By Lemma 2, (3.24) can be equivalently written as

$$x^\star = \mathbf{1}_n \bar{c} + J^{-1}(d-b)\bar{w}. \tag{3.25}$$

If the control input is applied to the misbehaving agent (i.e., $b = d$), then (3.17) immediately follows from (3.25). ■

Now, we investigate the case when the disturbance and the desired command are time-varying. For this purpose, consider the assistant state given in (3.18) with $u^*(t)$ (i.e., $\zeta(t) \triangleq \eta(t) + A_{\mathrm{g}}^{-1} B_{\mathrm{g}} u^*(t)$), where $\dot{u}^*(t)$ is a piecewise continuous function of time. By following the steps in the proof of Theorem 1, which is used to obtain (3.19), it can be easily shown that

$$\dot{\zeta}(t) = A_{\mathrm{g}}\zeta(t) + A_{\mathrm{g}}^{-1} B_{\mathrm{g}} \dot{u}^*(t), \quad \zeta(0) = \zeta_0, \quad t \geq 0. \tag{3.26}$$

Corollary 1. Let $\tilde{e}(t) \triangleq x(t) - J^{-1} \begin{bmatrix} \gamma_1 b & d-b \end{bmatrix} u^*(t)$. Then,

$$\tilde{e}(t) = C_{\mathrm{g}} \zeta(t), \tag{3.27}$$

where $C_{\mathrm{g}} = [I_n, 0]$.

Proof. We can simply rewrite the definition of $\tilde{e}(t)$ as

$$\tilde{e}(t) = C_{\mathrm{g}} \eta(t) - J^{-1} \begin{bmatrix} \gamma_1 b & d-b \end{bmatrix} u^*(t). \tag{3.28}$$

From (3.20), $x^\star = -C_{\mathrm{g}} A_{\mathrm{g}}^{-1} B_{\mathrm{g}} \bar{u}^*$. In conjunction with (3.24), this result implies that

$$C_{\mathrm{g}} A_{\mathrm{g}}^{-1} B_{\mathrm{g}} \bar{u}^* = -J^{-1} \begin{bmatrix} \gamma_1 b & d-b \end{bmatrix} \bar{u}^*, \quad \text{for all } \bar{u}^* \in \mathbb{R}^2. \tag{3.29}$$

Thus, $C_{\mathrm{g}} A_{\mathrm{g}}^{-1} B_{\mathrm{g}} = -J^{-1} \begin{bmatrix} \gamma_1 b & d-b \end{bmatrix}$. Now, (3.28) can be expressed as

$$\tilde{e}(t) = C_{\mathrm{g}} \eta(t) + C_{\mathrm{g}} A_{\mathrm{g}}^{-1} B_{\mathrm{g}} u^*(t). \tag{3.30}$$

Then, (3.27) follows immediately from (3.30). ■

Remark 2. Since A_g is Hurwitz, the system in (3.26) with $\dot{u}^*(t)$ viewed as input, is input-to-state stable. This implies that for any bounded $\dot{u}^*(t)$, $\zeta(t)$ is bounded. Hence, $\tilde{e}(t)$ is bounded by Corollary 1. This also implies that if $\lim_{t\to\infty}\dot{u}^*(t)=0$, then $\lim_{t\to\infty}\zeta(t)=0$ (e.g., see Exercise 4.58 in [22]). Thus, $\lim_{t\to\infty}\tilde{e}(t)=0$. Note that Theorem 1 is a special case of the second implication.

3.5 Discussion

In contrast to Theorem 1, this section proposes a graph-theoretical approach showing the steady-state value of each agent explicitly in the multiagent system whose graph topology is a tree, which henceforth refers to a fixed, connected, and undirected acyclic graph. This approach also shows that the largest steady-state deviation from the desired command in the multiagent system is minimized if the driver agent is located as close as possible to the misbehaving agent.

We now introduce a useful fact given by Theorem 1.5.1 in [43]: In a tree, there exists a unique path between any two vertices. This fact is extensively used in this section without explicitly mentioning it. Then, let $\mathcal{G}$ be a tree consisting of a driver agent and a misbehaving agent denoted by v_d and v_m, respectively.

For each $v_k \in V(P_{dm})$, define

$$V_k \triangleq \Big\{ \bigcup_{i=1}^{n} V(P_{ki}) : \; V(P_{ki}) \cap V(P_{dm}) = \{v_k\} \Big\}. \tag{3.31}$$

The next lemma verifies that the collection $\mathcal{P} \triangleq \{V_k : v_k \in V(P_{dm})\}$ gives a partition of $V(\mathcal{G})$.

Lemma 3. $\mathcal{P}$ satisfies the following properties

i) If $V_k \in \mathcal{P}$, then $v_k \in V_k$.

ii) If $V_j \in \mathcal{P}$ and $V_l \in \mathcal{P}$ with $j \neq l$, then $V_j \cap V_l = \emptyset$.

iii) $V(\mathcal{G}) = \bigcup_{V_k \in \mathcal{P}} V_k$.

Proof. The properties *i)* and *iii)* are trivial consequences of the given definition. For the property *ii)*, let $V_j \in \mathcal{P}$ and $V_l \in \mathcal{P}$ with $j \neq l$, but assume for contradiction that $V_j \cap V_l$ is nonempty. Then, let $v_r \in V_j \cap V_l$; hence, $v_r \in V_j$ and $v_r \in V_l$. By definition, $V(P_{jr}) \cap V(P_{dm}) = \{v_j\}$ and $V(P_{lr}) \cap V(P_{dm}) = \{v_l\}$. Note that $\{v_j, v_l\} \subseteq V(P_{jl}) \subseteq V(P_{dm})$. Now, observe that $P_{jl} \cup P_{lr} = P_{jr}$. Thus, $V(P_{jr}) \cap V(P_{dm}) = V(P_{jl})$. In conjunction with $V(P_{jr}) \cap V(P_{dm}) = \{v_j\}$, this implies that $\{v_j\} \supseteq \{v_j, v_l\}$, a contradiction. ■

Remark 3. For every $V_k \in \mathcal{P}$, let $S_k \triangleq V_k \setminus \{v_k\}$. By Lemma 3, *i)* $S_k = \emptyset$ if, and only if, $V_k = \{v_k\}$, *ii)* $S_j \cap S_l = \emptyset$ whenever $j \neq l$, *iii)* $S_k = V_k \setminus V(P_{dm})$, and *iv)* $S \triangleq \bigcup_k S_k = V(\mathcal{G}) \setminus V(P_{dm})$.

To present the main result of this section, given in Theorem 2, we need the following lemmas.

Lemma 4. If $V_k \in \mathcal{P}$, then $N(v_k) \cap S \subseteq S_k$.

Proof. Let $V_k \in \mathcal{P}$. Clearly, $v_k \in V(P_{dm})$. Fix $v_j \in N(v_k) \cap S$. Thus, $v_j \in N(v_k)$ and $v_j \notin V(P_{dm})$. Now, observe that $V(e_{kj}) \cap V(P_{dm}) = \{v_k\}$; hence, $v_j \in S_k$. ■

Lemma 5. Let $V_k \in \mathcal{P}$. If $v_r \in S_k$, then $N(v_r) \subseteq V_k$.

Proof. Let $v_r \in S_k$. By definition, $V(P_{kr}) \subseteq V_k$, $V(P_{kr}) \cap V(P_{dm}) = \{v_k\}$, and $r \neq k$. Assume, on the contrary, that there exists a $v_j \in N(v_r)$ such that $v_j \notin V_k$. Hence, $P_{kr} \cup e_{rj} = P_{kj}$ and $V(P_{kj}) \cap V(P_{dm}) = \{v_k, v_j\}$. This implies $V(e_{rj}) \cap V(P_{dm}) = \{v_j\}$. Now, there exists a $V_j \in \mathcal{P}$ such that $v_r \in S_j$, contradicting the fact that $S_k \cap S_j = \emptyset$. ■

Let us partition $x^\star$ in Theorem 1 as $x^\star = [x_1^\star, \ldots, x_n^\star]^{\mathrm{T}}$.

Theorem 2. Let $V_k \in \mathcal{P}$. If $v_i \in V_k$, then

$$x_i^\star = \bar{c} + d_{\mathcal{G}}(v_d, v_k)\bar{w}. \tag{3.32}$$

Proof. For each $v_i \in V_k$, let $\bar{x}_i \triangleq \bar{c} + d_{\mathcal{G}}(v_d, v_k)\bar{w}$. By means of Lemma 3, define $\bar{x} \triangleq [\bar{x}_1, \ldots, \bar{x}_n]^{\mathrm{T}}$. Then, the problem is to verify that $x^\star = \bar{x}$. Note that it is enough to prove this when $\bar{c} = 0$ and $\bar{w} = 1$. Since J is nonsingular, it is now enough to show that $J\bar{x} = d - b$.

We can always enumerate the vertices of $\mathcal{G}$ as follows: Let $v_d = v_1$ and $v_m = v_{|P_{dm}|}$. Let the vertices of P_{dm} be in ascending order from v_d to v_m; that is, $P_{dm} = v_1 v_2 \ldots v_m$. As a consequence of the enumeration, b is a unit vector with a 1 in the 1^{st} element and d is a unit vector with a 1 in the m^{th} element. Moreover, $J = \mathcal{L}(\mathcal{G}) + \mathrm{diag}(\gamma_1, 0, \ldots, 0)$.

Suppose first that S is nonempty. Let J_{a} and J_{b} be the matrices consisting of the first m rows of J and the last $n - m$ rows of J, respectively. They are denoted by

$$J_{\mathrm{a}} \triangleq \begin{bmatrix} — & J_1 & — \\ & \vdots & \\ — & J_m & — \end{bmatrix}, \quad J_{\mathrm{b}} \triangleq \begin{bmatrix} — & J_{m+1} & — \\ & \vdots & \\ — & J_n & — \end{bmatrix}.$$

Then, $J = [J_{\rm a}^{\rm T}, J_{\rm b}^{\rm T}]^{\rm T}$. Let also $b_{\rm a}$ be the vector that consists of the first m elements of $d-b$ so that $d-b = [b_{\rm a}^{\rm T}, 0]^{\rm T}$. Note that $J\bar{x} = d-b$ if, and only if, Claims 1 and 2 hold.

Claim 1. $J_{\rm a}\bar{x} = b_{\rm a}$.

Proof (Claim 1). Suppose $m > 2$. In this case, $b_{\rm a} = [-1, 0, \ldots, 0, 1]^{\rm T}$. First, let $v_r \in V(P_{dm}) \setminus \{v_1, v_m\}$. Thus, $V_r \in \mathcal{P}$ and $v_r \in V_r$, which implies $\bar{x}_r = d_{\mathcal{G}}(v_1, v_r) = r-1$. By Lemma 4, $N(v_r) \cap S \subseteq S_r$. Therefore, $\bar{x}_i = \bar{x}_r$ for all $v_i \in N(v_r) \cap S$. Next, observe that $N(v_r) \cap V(P_{dm}) = \{v_{r-1}, v_{r+1}\}$. Hence, $\bar{x}_{r-1} = r-2$ and $\bar{x}_{r+1} = r$. Now, $J_r\bar{x} = -\bar{x}_{r-1} + d_r\bar{x}_r - \bar{x}_{r+1} - (d_r - 2)\bar{x}_r$. This yields $J_r\bar{x}_r = 0$. Second, consider v_1. Then, $\bar{x}_1 = 0$. Similar to the first subcase, $\bar{x}_i = \bar{x}_1$ for all $v_i \in N(v_1) \cap S$. It is also noted that $N(v_1) \cap V(P_{dm}) = \{v_2\}$, which gives $\bar{x}_2 = 1$. Thus, $J_1\bar{x} = (d_1 + \gamma_1)\bar{x}_1 - \bar{x}_2 - (d_1 - 1)\bar{x}_1 = -1$. Third, consider v_m; hence, $\bar{x}_m = m-1$. In the same way as above, $\bar{x}_i = \bar{x}_m$ for all $v_i \in N(v_m) \cap S$. Also, $N(v_m) \cap V(P_{dm}) = \{v_{m-1}\}$, so $\bar{x}_{m-1} = m-2$. Thus, $J_m\bar{x} = -\bar{x}_{m-1} + d_m\bar{x}_m - (d_m - 1)\bar{x}_m = 1$. This completes the proof for the case $m > 2$.

Suppose $m \leq 2$. If $m = 2$, then $b_{\rm a} = [-1, 1]^{\rm T}$ and the result follows by only considering the first and the third subcases of the first case. If $m = 1$, the result can be easily verified. □

Claim 2. $J_{\rm b}\bar{x} = 0$.

Proof (Claim 2). Let $v_r \in S$. We assume, without loss of generality, that $v_r \in S_m$. But $N(v_r) \subseteq V_m$ by Lemma 5. Thus, $\bar{x}_i = \bar{x}_m$ for all $v_i \in N(v_r) \cup \{v_r\}$, so $J_r\bar{x} = 0$. □

Second, suppose that $S = \emptyset$. In this specific case, one can show that $J\bar{x} = d-b$ by following and simplifying the steps in the proof of Claim 1. ■

The next corollaries are now immediate.

Corollary 2. Let $\tilde{e}_i(t) \triangleq x_i(t) - \begin{bmatrix} 1 & d_{\mathcal{G}}(v_d, v_k) \end{bmatrix} u^*(t)$ for all $v_i \in V_k$. Then, $\tilde{e}(t)$ in Corollary 1 is equal to $[\tilde{e}_1(t), \ldots, \tilde{e}_n(t)]^{\rm T}$.

Corollary 3. Let $e_i^\star \triangleq x_i^\star - \bar{c}$. Then,

$$\max_{v_i \in V(\mathcal{G})} |e_i^\star| = d_{\mathcal{G}}(v_d, v_m)|\bar{w}|, \quad \operatorname*{argmax}_{v_i \in V(\mathcal{G})} |e_i^\star| = V_m, \tag{3.33}$$

$$\min_{v_i \in V(\mathcal{G})} |e_i^\star| = 0, \quad \operatorname*{argmin}_{v_i \in V(\mathcal{G})} |e_i^\star| = V_d. \tag{3.34}$$

3.6 Illustrative Numerical Examples

In this section, we present numerical examples to illustrate the implementation of theoretical results given in this paper. First, we reconsider the motivational example given in Section 3.3 to show the bound-

edness of the trajectory of each agent in the multiagent system if a control input is applied to any agent. To be consistent with the example in Section 3.3, node 16 denotes the misbehaving agent. For this example, we select node 4 as the driver agent. Next, the desired command is given as $\bar{c} = 5$ and the misbehaving agent is subject to the disturbance $w(t) = 1 + sin(t)$. We set the coefficients γ_1 and γ_2 as 1.

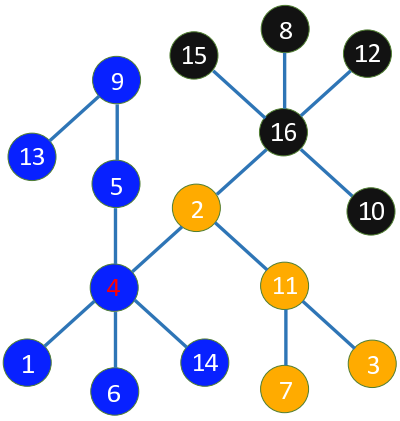

Figure 3.4: Color representation for each agent in Figure 3.5.

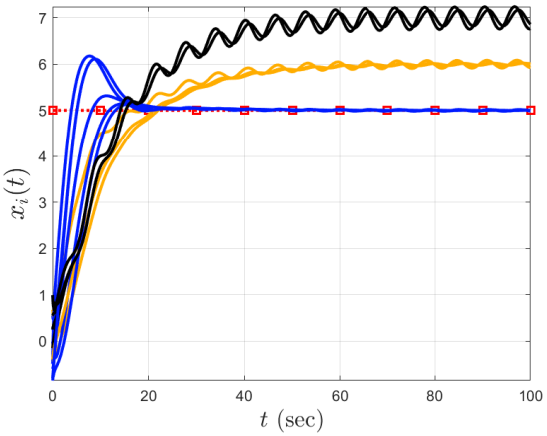

Figure 3.5: The trajectories of all agents in the multiagent system, where node 16 is subject to a disturbance and node 4 is injected a control input.

In contrast to the unboundedness of the trajectory of each agent in the example given in Section 3.3, the trajectories of all agents stay bounded since all conditions given in Remark 1 are satisfied. Figure 3.4 defines the color of each agent used in Figure 3.5, which depicts the trajectory of each agent. The trajectories of agents showing the similar response are painted by the same color in Figure 3.4.

In the following examples, we demonstrate the steady-state value of each agent by using Theorems 1 and 2 since the boundedness of the trajectory of each agent has already been shown by applying a control input to an agent in the system.

Consider the multiagent system with the graph topology given in Figure 3.1. In this example, we set the disturbance $w = 5$ and the desired command $c = 5$. In addition, the coefficients γ_1 and γ_2 are set as 1. Let the 5^{th} and 16^{th} nodes denote the driver and the misbehaving agents, respectively.

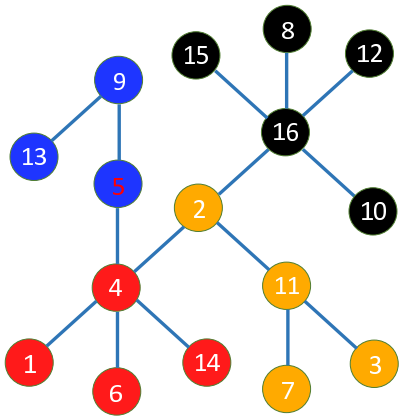

Figure 3.6: Color representation for each agent in Figure 3.7.

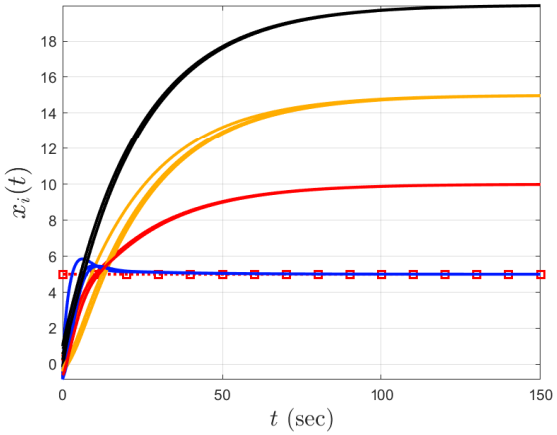

Figure 3.7: The trajectories and the steady-state values of all agents in the multiagent system, where node 16 is subject to a disturbance and node 5 is injected a control input.

The steady-state values of all agents are obtained by using Theorem 1. If we apply the formula given in (3.16), then the steady-state values of all agents are obtained as $x_{16}^\star = x_8^\star = x_{10}^\star = x_{12}^\star = x_{15}^\star = 20$, $x_2^\star = x_3^\star = x_7^\star = x_{11}^\star = 15$, $x_4^\star = x_1^\star = x_6^\star = x_{14}^\star = 10$, $x_5^\star = x_9^\star = x_{13}^\star = 5$. Figure 3.6 defines the color of each agent used in Figure 3.7, which depicts the trajectory and the steady-state value of each agent. Similarly,

agents having almost identical trajectories are painted by the same color. The steady-state value of each agent obtained by Theorem 1 satisfies the one shown in Figure 3.7.

In the last example, we reconsider the multiagent system with the graph topology given in Figure 3.1 to obtain the steady-state value of each agent by Theorem 2. In this case, let the 9^{th} and 16^{th} nodes be the driver and the misbehaving agents, respectively. The disturbance $\bar{w}$ and the desired command $\bar{c}$ are set as $\bar{w} = 3$ and $\bar{c} = 7$. Let coefficients γ_1 and γ_2 be 1.

We enumerate vertices of $\mathcal{G}$ as desired in Theorem 2. Then Figure 3.1 turns into Figure 3.8. Therefore, nodes 9, 5, 4, 2, and 16 in Figure 3.1 are represented by nodes 1, 2, 3, 4, and 5 in Figure 3.8. After this point, we recall nodes with numbers as given in Figure 3.8.

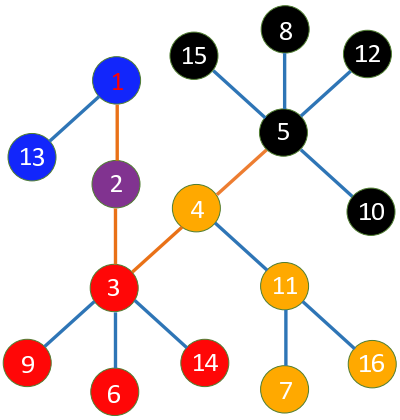

Figure 3.8: Color representation for each agent in Figure 3.9.

Now, nodes 1 and 5 denote the driver and the misbehaving agents in Figure 3.8, respectively. The path P_{15} (i.e., P_{dm}) from v_1 to v_5 is shown by the orange line and the set of vertices on this path is $V(P_{15}) = \{v_1, v_2, v_3, v_4, v_5\}$. By definition, $V_1 = \{v_{13}\}$, $V_2 = \{\emptyset\}$, $V_3 = \{v_6, v_9, v_{14}\}$, $V_4 = \{v_7, v_{11}, v_{16}\}$, and $V_5 = \{v_8, v_{10}, v_{12}, v_{15}\}$. By Theorem 2, the steady-state value of each agent $v_i \in V(P_{dm})$ is obtained as $x_1^\star = 7$, $x_2^\star = 10$, $x_3^\star = 13$, $x_4^\star = 16$, and $x_5^\star = 19$. Similarly, the steady-state value of each agent in the set S is obtained as $x_{13}^\star = 7$, $x_6^\star = x_9^\star = x_{14}^\star = 13$, $x_7^\star = x_{11}^\star = x_{16}^\star = 16$, and $x_8^\star = x_{10}^\star = x_{12}^\star = x_{15}^\star = 19$. The steady-state value of each agent obtained from (3.16), (3.32), and Figure 3.9 gives the same result as expected in this example.

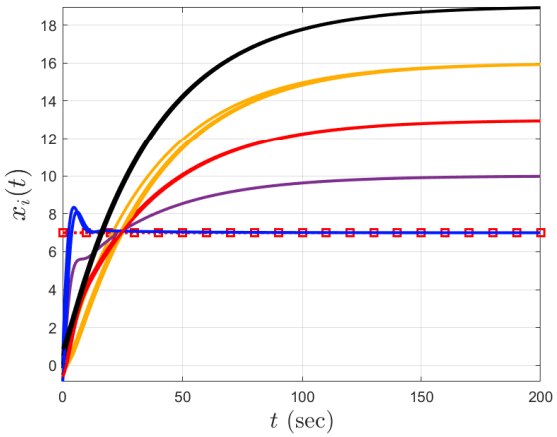

Figure 3.9: The trajectories and the steady-state values of all agents in the multiagent system, where node 5 is subject to a disturbance and node 1 is injected a control input.

3.7 Conclusions

In this paper, we have studied the stability analysis of the multiagent system in the presence of only the misbehaving agent and both the misbehaving and the driver agents. It has been shown that the proposed a proportional integral controller for the driver agent in the multiagent system subject to a disturbance makes the resulting closed-loop system matrix of the multiagent system Hurwitz. Then, we demonstrate two methods to calculate the steady-state value of each agent in the multiagent system whose graph topology for the first method is fixed, connected and undirected and for the second method is a tree. Lastly, we also propose a way to show that the largest steady-state deviation from the desired command in the multiagent system is minimized if the driver agent is located as close as possible to the misbehaving agent.

We have identified some potential future research directions. We believe that there would be a good possibility to extend Theorem 2 to graph topologies that consist of cycles without violating the uniqueness of the path P_{dm} owing to the simulation results. In addition, we will investigate multiagent systems in the presence of multiple misbehaving agents with certain number of driver agents.

CHAPTER 4: CONCLUDING REMARKS AND FUTURE RESEARCH

4.1 Concluding Remarks

The research reported in this thesis has shown the experimental validation of recently proposed distributed adaptive control architecture for a class of heterogeneous uncertain multiagent systems. In addition, a proportional integral controller for a driver agent in the multiagent system having limited resources in the presence of a disturbance has been proposed with stability analyses.

Specifically, we used the distributed adaptive control architecture proposed in [15], which has a nominal part and an adaptive augmentation part for each agent to suppress the effect of uncertainties and disturbances effectively in our experiment. In our experimental results, we observed that the output of the leader is followed by the output of agents the with huge amplitude of oscillations comparing to the control input with adaptive augmentation. Moreover, the effect of uncertainties were minimized and the output of the leader was followed by the output of agents with considerably lower amplitude of oscillations by turning on the adaptive augmentation. These observations coincide with the theoretical results in [15]. We also provided experimental plots to show the efficacy of the proposed distributed adaptive control architecture.

Due to some limitations of using the control architecture similar to [15] in some real-life scenarios, we proposed a proportional integral controller in Chapter 3, which makes the resulting closed-loop system matrix of the multiagent system Hurwitz. Therefore, the trajectories of all agents in the multiagent system with a fixed, connected, and undirected graph, where the system is subject to a bounded disturbance through an agent (i.e., misbehaving agent), remain bounded with only one control input having a bounded command irrespective of which agent we apply the control input. We then showed the steady-state value of each agent based on the control input is applied to the undisturbed and disturbed agent, respectively. Moreover, a graph-theoretical approach is derived to show the steady-state value of each agent in the multiagent system whose graph topology is a fixed tree. This approach provides a way to show that the largest steady-state deviation from the desired command in the multiagent system is minimized if the driver agent is located as

close as possible to the misbehaving agent. We also presented several numerical examples to illustrate the implementation of the theoretical results.

4.2 Future Research

In this section, there are some research directions and suggestions that can be considered for future work related to the results in this thesis. In addition to the experiment presented in Chapter 2, additional experimentation with more complex systems could be conducted in order to show the effectiveness of the distributed adaptive control architecture. While the results in Chapter 3 derived for a multiagent system subject just a single control input and a disturbance, this can be extended to multiple control inputs with disturbances. This can also be considered from the optimality perspective such as deciding optimal number of control inputs to suppress the effect of disturbances. Lastly, some experiments can be conducted to bridge the gap between theory and practice.

REFERENCES

[1] *Quanser IP02 Linear Inverted Pendulum User Manual*, 2012. Available at https://www.quanser.com/products/linear-servo-base-unit-inverted-pendulum/.

[2] Y. Cao, W. Yu, W. Ren, and G. Chen, "An overview of recent progress in the study of distributed multi-agent coordination," *IEEE Transactions on Industrial Informatics*, vol. 9, no. 1, pp. 427–438, 2013.

[3] Y. Hong, G. Chen, and L. Bushnell, "Distributed observers design for leader-following control of multi-agent networks," *Automatica*, vol. 44, pp. 846–850, 2008.

[4] K. K. Oh, M. C. Park, and H. S. Ahn, "A survey of multi-agent formation control," *Automatica*, vol. 53, pp. 424–440, 2015.

[5] A. Jadbabaie, J. Lin, and A. S. Morse, "Coordination of groups of mobile autonomous agents using nearest neighbor rules," *IEEE Transactions on Automatic Control*, vol. 48, pp. 988–1001, 2003.

[6] R. Olfati-Saber and R. M. Murray, "Consensus problems in networks of agents with switching topology and time-delays," *IEEE Transactions on Automatic Control*, vol. 49, pp. 1520–1533, 2004.

[7] W. Ni and D. Cheng, "Leader-following consensus of multi-agent systems under fixed and switching topologies," *Systems & Control Letters*, vol. 59, pp. 209–217, 2010.

[8] M. Ji, M. Ferrari-Trecate, M. Egerstedt, and A. Buffa, "Containment control in mobile networks," *IEEE Transactions on Automatic Control*, vol. 53, no. 8, pp. 1972–1975, 2008.

[9] G. Notarstefano, M. M. Egerstedt, and M. Haque, "Containment in leader-follower networks with switching communication topologies," *Automatica*, vol. 47, pp. 1035–1040, 2011.

[10] W. Ren and R. W. Beard, "Decentralized scheme for spacecraft formation flying via the virtual structure approach," *AIAA Guidance, Navigation, and Control Conference*, vol. 27, no. 1, pp. 73–82, 2004.

[11] M. Basiri, A. N. Bishop, and P. Jensfelt, "Distributed control of triangular formations with angle-only constraints," *Systems & Control Letters*, vol. 59, pp. 147–154, 2010.

[12] H. Zhang and F. L. Lewis, "Adaptive cooperative tracking control of higher-order nonlinear systems with unknown dynamics," *Automatica*, vol. 48, pp. 1432–1439, 2012.

[13] T. Yucelen and E. N. Johnson, "Control of multivehicle systems in the presence of uncertain dynamics," *International Journal of Control*, vol. 86, no. 9, pp. 1540–1553, 2013.

[14] T. Yucelen and E. N. Johnson, "Cooperative control of uncertain multivehicle systems," *IEEE Conference on Decision and Control*, pp. 837–842, 2012.

[15] S. B. Sarsilmaz, T. Yucelen, and T. Oswald, "A distributed adaptive control approach for heterogeneous uncertain multiagent systems," *AIAA Guidance, Navigation, and Control Conference*, 2018.

[16] P. Michiardi and R. Molva, "Core: A collaborative reputation mechanism to enforce node cooperation in mobile ad hoc network," *Advanced Communications and Multimedia Security Conference*, pp. 107–121, 2002.

[17] G. De La Torre and T. Yucelen, "Adaptive architectures for resilient control of networked multiagent systems in the presence of misbehaving agents," *International Journal of Control*, vol. 91, no. 3, pp. 495–507, 2018.

[18] Z. Li, Z. Duan, L. Xie, and X. Liu, "Distributed robust control of linear multi-agent systems with parameter uncertainties," *International Journal of Control*, vol. 85, no. 8, pp. 1039–1050, 2012.

[19] E. Soltanmohammadi, M. Orooji, and M. Narangi-Pour, "Decentralized hypothesis testing in wireless sensor networks in the presence of misbehaving nodes," *IEEE Transactions on Information Forensics and Security*, vol. 8, no. 1, pp. 205–215, 2013.

[20] M. Franceschelli, A. Giua, and C. Seatzu, "Decentralized fault diagnosis for sensor networks," *IEEE International Conference on Automation Science and Enginering*, pp. 334–339, 2009.

[21] E. Yildirim, S. Sarsilmaz, and T. Yucelen, "Application of a distributed adaptive control approach to a heterogeneous multiagent mechanical platform," *AIAA Guidance, Navigation, and Control Conference*, 2019.

[22] H. K. Khalil, *Nonlinear systems*. Prentice Hall, 2002.

[23] F. L. Lewis, H. Zhang, K. Hengster-Movric, and A. Das, *Cooperative control of multi-agent systems Optimal and adaptive design approaches*. Springer, 2014.

[24] E. Lavretsky and K. A. Wise, *Robust and adaptive control with aerospace applications*. Springer-Verlag, 2013.

[25] S. B. Sarsilmaz and T. Yucelen, "A distributed control approach for heterogeneous multiagent systems (under review)," *Automatica*.

[26] J. Huang, *Nonlinear output regulation problem: Theory and applications*. SIAM, 2004.

[27] C. Huang and X. Ye, "Cooperative output regulation of heterogeneous multi-agent systems: an H_∞ criterion," *IEEE Transactions on Automatic Control*, vol. 59, no. 1, pp. 267–273, 2014.

[28] S. A. Campbell, S. Crawford, and K. Morris, "Friction and the inverted pendulum stabilization problem," *ASME Dynamic Systems and Control Conference*, 2008.

[29] M. Mesbahi and M. Egerstedt, *Graph theoretic methods in multiagent networks*. Princeton University Press, 2010.

[30] R. Olfati-Saber, J. A. Fax, and R. M. Murray, "Consensus and cooperation in networked multi-agent systems," *Proceedings of IEEE*, vol. 95, no. 1, pp. 215–233, 2007.

[31] T. Yucelen and M. Egerstedt, "Control of multiagent systems under persistent disturbances," *IEEE American Control Conference*, pp. 5264–5269, 2012.

[32] W. Cao, J. Zhang, and W. Ren, "Leader-follower consensus of linear multi-agent systems with unknown external disturbances," *Systems & Control Letters*, vol. 82, pp. 64–70, 2015.

[33] G. S. Seyboth and F. Allgower, "Output synchronization of linear multi-agent systems under constant disturbances via distributed integral action," *IEEE American Control Conference*, pp. 62–67, 2015.

[34] O. Manolov, S. Noykov, B. Iske, J. Klahold, G. Georgiev, U. Witkowski, and U. Ruckert, "Gard- an intelligent system for distributed exploration of landmine fields simulated by a team of khepera robots," *International Conference Automatics And Informatics*, vol. 1, pp. 199–202, 2003.

[35] H. Cruz, M. Eckert, J.-F. Meneses, and J. Martinez, "Effecient forest fire detection index for application in unmanned aerial systems," *Sensors*, vol. 16, no. 6, p. 893, 2016.

[36] A. R. Girard, A. S. Howell, and J. K. Hedrick, "Border patrol and surveillance missions using multiple unmanned air vehicles," *IEEE Conference on Decision and Control*, pp. 620–625, 2004.

[37] K. Alexis, A. Nikolakopoulos, A. Tzes, and L. Dritsas, "Coordination of helicopter uavs for aerial forest-fire surveillance," *Applications of Intelligent Control to Engineering Systems*, pp. 169–193, 2009.

[38] Y. Liu, H. Xin, Z. Qu, and D. Gan, "An attack-resilient cooperative control strategy of multiple distributed generators in distibution networks," *IEEE Transactions Smart Grid*, vol. 7, no. 6, pp. 2923–2932, 2016.

[39] W. Zeng and M.-Y. Zhang, Y. Chow, "Resilient distributed energy management subject to unexpected misbehaving generation units," *IEEE Transactions on Industrial Informatics*, vol. 13, no. 1, pp. 208–216, 2016.

[40] O. Mason and V. M., "Graph theory and networks in biology," *IET Systems Biology*, vol. 1, no. 2, pp. 89–119, 2007.

[41] A. Raj and F. Powell, "Models of network spread and network degenaration in brain disorders," *Biological Psychiatry*, vol. 3, pp. 788–797, 2018.

[42] O. Sporns, "From simple graphs to the connectome: Networks in neuroimaging," *Neuoreimage*, vol. 62, pp. 881–886, 2012.

[43] R. Diestel, *Graph Theory*. Springer, 2005.

[44] O. Bretscher, *Linear Algebra with Applications*. Pearson, 2009.

[45] D. S. Bernstein, *Matrix Mathematics: Theory, Facts, and Formulas*. Princeton University Press, 2009.

[46] S. B. Sarsilmaz and T. Yucelen, "A distributed control approach for heterogeneous linear multiagent systems," *arXiv preprint arXiv:1901.02600*, 2019.

APPENDIX A: ERRATA LIST

The reference [25] given in footnote 1 in Chapter 2 is replaced with [46].

APPENDIX B: COPYRIGHT PERMISSION

The permission below is for the use of material in Chapter 2.

Emre Yildirim <emreyildirim@mail.usf.edu>

Permission for a conference paper

4 messages

Emre Yildirim <emreyildirim@mail.usf.edu> Tue, Mar 19, 2019 at 1:37 PM
To: heatherb@aiaa.org

Hello Heather,

My name is Emre YILDIRIM. I am a master student in Mechanical Engineering at the University of South Florida. I would like to use the paper I published in January 2019 at AIAA Conference in my thesis. The title of my paper is " Application of a Distributed Adaptive Control Approach to a Heterogeneous Multiagent Mechanical Platform". I would like to request permissions for using this paper in my thesis.

Best Regards,

Emre.

Sender notified by
Mailtrack

Heather Brennan <HeatherB@aiaa.org> Tue, Mar 19, 2019 at 1:48 PM
To: Emre Yildirim <emreyildirim@mail.usf.edu>

Dear Emre,

Thanks for your inquiry. You and your coauthors retained copyright to the conference paper that was presented at the AIAA forum in January. Therefore, because AIAA is not the copyright owner, you do not need to seek permission to republish the work. Please do acknowledge prior publication of your conference paper within the main text or as a footnote to this section/chapter of your thesis, as appropriate (e.g., “This section is reprinted from [paper title and authors].”) and fully cite the original source in your reference list.

If you have any further questions, please let me know.

Sincerely,

Heather A. Brennan

Director, Publications

-

American Institute of Aeronautics and Astronautics www.aiaa.org
12700 Sunrise Valley Drive, Suite 200